Role of p38 Mitogen-Activated Protein Kinase Activation in Podocyte Injury and Proteinuria in Experimental Nephrotic Syndrome

Masao Koshikawa,* Masashi Mukoyama,* Kiyoshi Mori,* Takayoshi Suganami,* Kazutomo Sawai,* Tetsuro Yoshioka,* Tetsuya Nagae,* Hideki Yokoi,* Hiroshi Kawachi,† Fujio Shimizu,† Akira Sugawara,* and Kazuwa Nakao*

**Department of Medicine and Clinical Science, Kyoto University Graduate School of Medicine, Kyoto, and †Department of Cell Biology, Institute of Nephrology, Niigata University Graduate School of Medical and Dental Sciences, Niigata, Japan*

Podocytes play an important role in maintaining normal glomerular function and structure, and podocyte injury leads to proteinuria and glomerulosclerosis. The family of mitogen-activated protein kinases (MAPK; extracellular signal-regulated kinase [ERK], c-Jun N-terminal kinase, and p38) may be implicated in the progression of various glomerulopathies, but the role of MAPK in podocyte injury remains elusive. This study examined phosphorylation of p38 MAPK in clinical glomerulopathies with podocyte injury, as well as in rat puromycin aminonucleoside (PAN) nephropathy and mouse adriamycin (ADR) nephropathy. The effect of treatment with FR167653, an inhibitor of p38 MAPK, was also investigated in rodent models. In human podocyte injury diseases, the increased phosphorylation of p38 MAPK was observed at podocytes. In PAN and ADR nephropathy, the phosphorylation of p38 MAPK and ERK was marked but transient, preceding overt proteinuria. Pretreatment with FR167653 (day −2 to day 14, subcutaneously) to PAN or ADR nephropathy completely inhibited p38 MAPK activation and attenuated ERK phosphorylation, with complete suppression of proteinuria. Electron microscopy and immunohistochemistry for nephrin and connexin43 revealed that podocyte injury was markedly ameliorated by FR167653. Furthermore, early treatment with FR167653 effectively prevented glomerulosclerosis and renal dysfunction in the chronic phase of ADR nephropathy. In cultured podocytes, PAN or oxidative stress induced the phosphorylation of p38 MAPK along with actin reorganization, and FR167653 inhibited such changes. These findings indicate that the activation of MAPK is necessary for podocyte injury, suggesting that p38 MAPK and, possibly, ERK should become a potential target for therapeutic intervention in proteinuric glomerulopathies.

J Am Soc Nephrol 16: 2690–2701, 2005. doi: 10.1681/ASN.2004121084

Podocytes are highly differentiated cells that form multiple interdigitating foot processes (1). They are interconnected by slit diaphragms and cover the glomerular basement membrane (GBM) surface. They stabilize glomerular architecture by counteracting the distension of the capillary wall and GBM (1) and maintain a large filtration surface through the slit diaphragms (2). Podocytes contribute to the specific size and charge filtration barrier, and their damage leads to the retraction of their foot processes and proteinuria (3,4).

Human acquired proteinuric glomerulopathies, such as minimal-change nephrotic syndrome (MCNS), focal segmental glomerulosclerosis (FSGS), and membranous nephropathy (MN), commonly exhibit foot process effacement of podocytes and loss of slit diaphragms in electron microscopy; these glomerulopathies therefore are considered as podocyte injury diseases (podocytopathies) (5). Several experimental models, such as rat puromycin aminonucleoside (PAN) nephropathy (6) and mouse adriamycin (ADR) nephropathy (7) that develop massive proteinuria resembling human minimal change disease, have provided insights into the cellular and intracellular mechanisms of podocyte injury disease. Recent advances coupled with molecular approaches have revealed crucial roles of slit diaphragm–associated proteins, including nephrin and podocin, in not only congenital but also acquired forms of proteinuric disorders (8,9). These studies have investigated the process or consequence of podocyte injury, but the mechanistic link between the pro-proteinuric insults and morphologic or functional impairment of podocytes remains to be fully understood.

The family of mitogen-activated protein kinases (MAPK), consisting of extracellular signal-regulated kinase (ERK), c-Jun N-terminal kinase (JNK), and p38, are activated by various extracellular stimuli, including growth factors and environmental stresses (10). The MAPK pathways involve multiple phosphorylation cascades, each of which mediates different signaling events either alone or in concert with other pathways (10). Especially, p38 MAPK is postulated to play a critical role

Received December 14, 2004. Accepted May 31, 2005.

Published online ahead of print. Publication date available at www.jasn.org.

Address correspondence to: Dr. Masashi Mukoyama, Department of Medicine and Clinical Science, Kyoto University Graduate School of Medicine, 54 Shogoin Kawahara-cho, Sakyo-ku, Kyoto 606-8507, Japan. Phone: +81-75-751-4285; Fax: +81-75-771-9452; E-mail: muko@kuhp.kyoto-u.ac.jp

ISSN: 1046-6673/1609-2690

in producing proinflammatory cytokines (11), mediating cell survival or apoptosis (12), and regulating the stability of cytoskeleton (13). These notions have prompted us to investigate the role of p38 MAPK in podocyte injury.

In this study, we investigated the alteration of p38 MAPK in disease states and reveal the activation of p38 MAPK at podocytes in clinical and experimental nephrotic syndromes, specifically from the preproteinuric state in the latter. Furthermore, we demonstrate that the treatment with FR167653, an inhibitor of p38 MAPK, in PAN nephropathy and ADR nephropathy completely abolishes proteinuria and prevents podocyte injury, suggesting that p38 MAPK activation is a common upstream mechanism necessary for podocyte injury in proteinuric glomerulopathies.

Materials and Methods

Antibodies

Primary antibodies used for Western blotting and immunohistochemical studies were rabbit anti–p38 MAPK, rabbit anti–phospho–p38 MAPK, rabbit anti-ERK, rabbit anti–phospho-ERK (Cell Signaling Technology, Boston, MA), rabbit anti-JNK, mouse anti–phospho-JNK (Santa Cruz Biotechnology, Santa Cruz, CA), mouse anti-nephrin (14), rabbit anti-nephrin (8), rabbit anti-connexin43 (Sigma, St. Louis, MO), mouse anti-synaptopodin (Progen, Heidelberg, Germany), and rabbit anti–TGF-β1 (Santa Cruz Biotechnology) antibodies.

Human Tissue Samples

Tissue samples were obtained at diagnostic renal biopsy performed at Kyoto University Hospital. We investigated the samples from patients who had MCNS, MN, and FSGS and were manifesting nephrotic-range proteinuria. As control human samples, we used nontumor tissues of the kidney from patients who had renal cell carcinoma and underwent nephrectomy or biopsy samples from the patients with minor glomerular abnormalities. The study was conducted under informed consent and was approved by the ethics committee on human research of Kyoto University Graduate School of Medicine.

Animal Experiments

All animal experiments were conducted in accordance with our institutional guidelines for animal research. For inducing rat PAN nephropathy, male Wistar-Kyoto rats that weighed 180 to 200 g received an intravenous injection of 50 mg/kg body wt PAN (Sigma) diluted in 0.9% saline. For inducing mouse ADR nephropathy, male BALB/c mice that weighed 20 to 25 g received an intravenous injection of 10 mg/kg body wt doxorubicin hydrochloride (Sigma) diluted in 0.9% saline. Control animals received vehicle only. Administration of FR167653 (Fujisawa Pharmaceutical, Osaka, Japan), a specific p38α MAPK inhibitor (15), was performed by subcutaneous injection (16) at a dose of 33 mg/kg body wt diluted in 0.5% methylcellulose (Sigma) daily from day −2 to day 14. In another series of experiments, daily FR167653 injection was started 10 min or 4 h after induction of the disease and continued for 2 wk (from day 0 to day 14) in these models. Control animals received an injection of methylcellulose alone.

Animals were fed a standard diet and given water *ad libitum*. We maintained these animals under alternating 12-h cycles of light and dark. Animals were killed on determined days after induction of the disease. Kidneys were harvested immediately for histologic and Western blot analyses.

Measurement of Blood and Urine Samples

Blood samples were obtained at the time of killing, and serum creatinine levels were measured using a kit (Wako, Osaka, Japan). For urine measurements, each animal was housed separately in a metabolic cage (Shinano Manufacturing, Tokyo, Japan) and daily urine volume was measured. Urinary albumin excretion was assayed with a rat or murine albumin ELISA kit (Exocell, Philadelphia, PA) (17).

Renal Histology and Electron Microscopy

Kidney sections were fixed with 4% buffered formaldehyde and embedded in paraffin as described (17,18). One-micrometer-thick sections were stained with periodic acid-Schiff and examined by light microscopy. Occurrence of the sclerotic glomeruli per section was assessed by counting the total number of glomeruli in a representative section from each sample. The procedure was performed by two investigators without knowledge of the origin of the slides, and the mean values were calculated.

For electron microscopy, small blocks of kidneys were fixed in 2.5% buffered glutaraldehyde, postfixed in 2% osmium tetroxide, dehydrated in graded ethanol, and embedded in epoxy resin (19). Ultrathin sections (0.1 μm thick) were stained with uranyl acetate and lead citrate and examined in an electron microscope (H-7600; Hitachi, Tokyo, Japan) at 75 kV.

Immunohistochemistry

For immunohistochemistry of phospho–p38 MAPK, kidney samples were fixed with 4% paraformaldehyde and embedded in paraffin. Three-micrometer sections were deparaffinized and rehydrated. Sections were treated with 0.3% H_2O_2 in methanol for 15 min to quench endogenous peroxide activity and were boiled at 100°C for 10 min in 10% citrate buffer to unmask antigens. Sections were incubated with anti–phospho–p38 MAPK at 4°C overnight and visualized using Vectastain ABC kit (Vector Laboratories, Burlingame, CA). Sections were counterstained with hematoxylin.

For immunofluorescence studies of nephrin and TGF-β1, 3-μm cryostat sections fixed with acetone were incubated for 1 h at 22°C with primary antibodies and stained with FITC-labeled anti-mouse or anti-rabbit IgG (Jackson Immunoresearch, West Grove, PA). For double staining of connexin43 and synaptopodin, sections were incubated with mixed primary antibodies and stained with FITC-labeled anti-rabbit IgG and TRITC-labeled anti-mouse IgG (Jackson Immunoresearch). Slides were examined with a confocal laser microscope (LSM5Pascal; Carl Zeiss, Munich, Germany) (19).

Western Blot Analysis

Glomeruli were isolated from the animals by graded sieving method (20). Western blot analysis was performed as described (17,18). In brief, isolated glomeruli or cells were lysed on ice in RIPA buffer that contained 10 μg/ml aprotinin, 2 mM dithiothreitol, 2 mM sodium orthovanadate, and 1 mM PMSF. Lysates were centrifuged at 15,000 rpm, and supernatants (50 μg protein/lane) were separated by 12.5% SDS-PAGE and transferred onto Immobilon filter (Millipore, Bedford, MA). After incubation with primary antibodies, immunoblots were developed with horseradish peroxidase–conjugated donkey anti-rabbit IgG (Amersham, Arlington Heights, IL) and a chemiluminescence kit (ECL plus; Amersham).

Cell Culture

A conditionally immortalized mouse podocyte cell line was provided by Dr. Peter Mundel (Albert Einstein College of Medicine, New York, NY) (21) and cultured as described (20). In brief, the cells were main-

tained at 33°C on dishes that were coated with collagen I (Koken, Tokyo, Japan), in RPMI 1640 medium (Nihonseiyaku, Tokyo, Japan) that contained 10% FBS (Sanko Junyaku, Tokyo, Japan) with 10 U/ml IFN-γ (Life Technologies BRL, Grand Island, NY). For differentiating podocytes, cells were cultured at 37°C with 5% FBS without IFN-γ for 2 wk. For experiment, cells were made quiescent in medium that contained 0.5% BSA (Sigma) for 24 h, pretreated with 10 μM FR167653 or vehicle 1 h before stimulation with 50 μg/ml PAN or 0.5 mM H_2O_2, and harvested at determined time after stimulation.

For analyzing actin cytoskeleton of cultured podocytes, cells were cultured on collagen I–coated coverslips in six-well dishes. For observation of F-actin filament, cells were fixed with 4% paraformaldehyde, incubated with 0.1% Triton X-100 for 10 min, and stained with 1 μM FITC-conjugated phalloidin (Sigma) for 30 min in darkness (21). Cover glasses were mounted, and the slides were examined by fluorescence microscopy.

Statistical Analyses

Data are expressed as means ± SEM. Statistical analysis was performed using ANOVA followed by Scheffe test. $P < 0.05$ was considered statistically significant.

Results

Enhanced Phosphorylation of p38 MAPK in Human and Rodent Podocyte Injury Diseases

In normal human kidneys, only a faint staining for phosphorylated p38 MAPK was observed in the glomeruli, mostly in the epithelial cells (Figure 1A). In proteinuric disorders, however, enhanced phosphorylation of p38 MAPK was detected at podocytes, as well as in parietal epithelial cells, as demonstrated in the biopsy specimens from the patients with MCNS (Figure 1B), MN (Figure 1C), and FSGS (Figure 1D). The mean occurrence of phospho–p38 MAPK–positive cells among nucleated cells per glomerulus (excluding parietal epithelial cells) was 5.2 ± 0.6, 11.1 ± 2.8, 18.2 ± 4.4, and 14.7 ± 4.8% in the samples from control kidney, MCNS, MN, and FSGS, respectively ($n = 3$ each).

We next examined rodent models of nephrotic syndrome. We found a marked increase of phosphorylated p38 MAPK in the isolated glomeruli of PAN nephropathy as well as ADR nephropathy on day 1 and day 3 (Figure 2, A and B), when urinary albumin excretion was still within normal range (see Figure 3, C and D). Enhanced phospho–p38 MAPK was confined mostly to podocytes (Figure 2, C and D). The mean occurrence of phospho–p38 MAPK–positive cells per glomerulus was 19.3 ± 1.9 and 16.7 ± 2.9% on day 1 in PAN and ADR nephropathy, respectively ($n = 4$ each). Thereafter, the levels of phospho–p38 MAPK got decreased and returned near the basal levels on day 7. We also examined the activation of other members of the MAPK family in these models of nephrotic syndrome. Phosphorylation of ERK (ERK-1 and -2) was increased in the glomeruli of PAN nephropathy on day 1 and day 3 and decreased on day 7, at a time course similar to that of p38 MAPK but with less pronounced activation (Figure 2E). Phosphorylation of JNK (JNK-1 and -2) was observed in the control glomeruli and unaltered during the course (Figure 2E). Essentially identical results for ERK and JNK changes were obtained in ADR nephropathy (data not shown). These findings indicate that p38 MAPK is markedly but transiently activated at podocytes before the appearance of overt proteinuria in rodent models of podocyte injury disease.

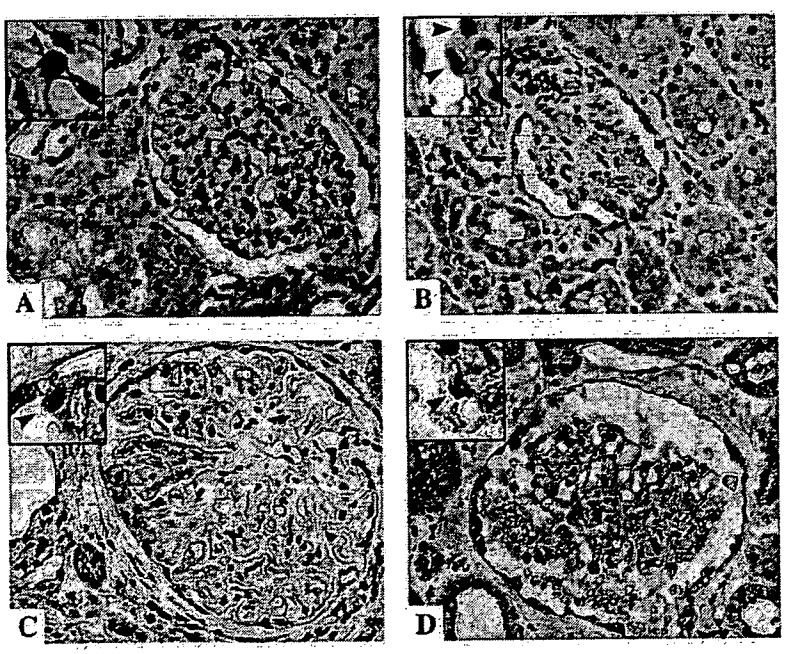

Figure 1. Phosphorylation of p38 mitogen-activated protein kinase (MAPK) in human glomerulopathies with podocyte injury. (A) In normal glomerulus, a weak staining for phospho–p38 MAPK was observed (arrowhead in inset). Enhanced phosphorylation of p38 MAPK was detected at nuclei of podocytes (arrowheads in insets) in the biopsy specimens from minimal-change disease (B), membranous nephropathy (C), and focal segmental glomerulosclerosis (D). Magnification, ×400; inset ×1000.

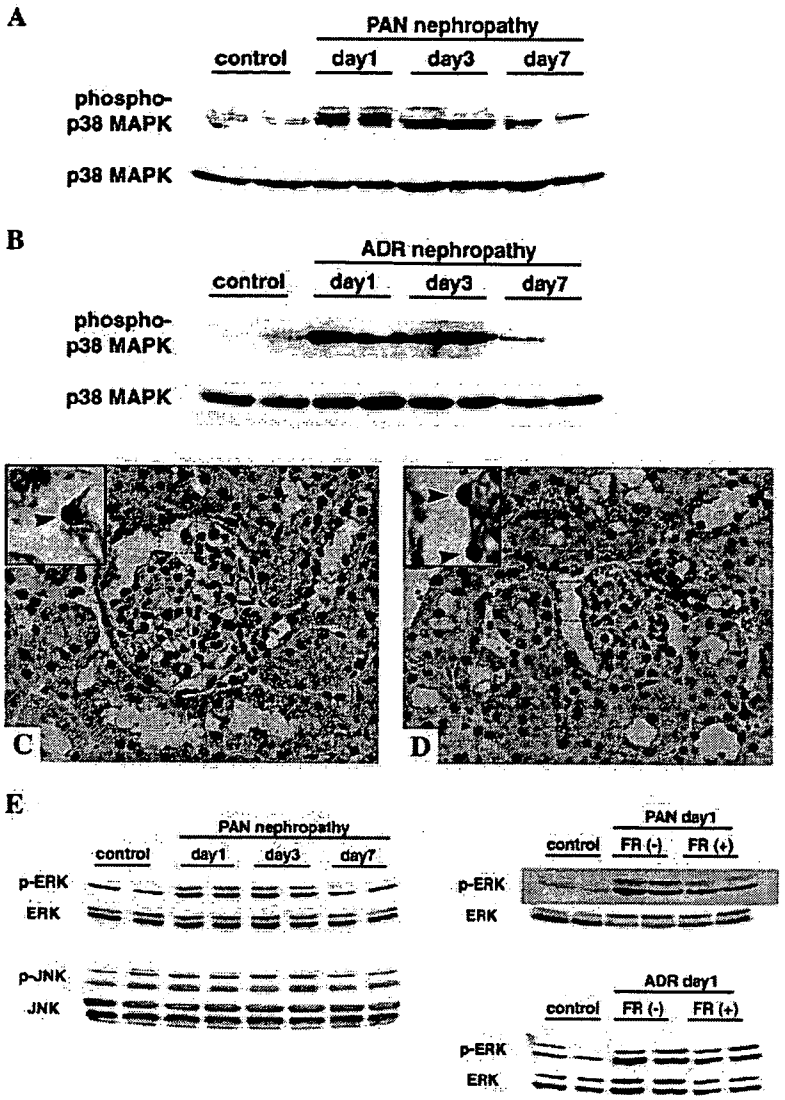

Figure 2. Phosphorylation of p38 MAPK in rat puromycin aminonucleoside (PAN) nephropathy and mouse adriamycin (ADR) nephropathy. Western blotting for phosphorylated p38 MAPK in glomeruli of rat PAN nephropathy (A) and mouse ADR nephropathy (B) revealed a marked increase on day 1 and day 3 and a significant decrease to almost basal levels on day 7. Blotting for total p38 MAPK was performed as internal control. Immunohistochemistry for phospho–p38 MAPK on day 1 of PAN nephropathy (C) and ADR nephropathy (D) revealed that enhanced phospho–p38 MAPK was confined mostly to podocytes (arrowheads). (E, Left) Western blotting for phosphorylated p44 and p42 extracellular signal-regulated kinase (ERK; ERK-1 and -2) and phosphorylated p46 and p54 c-Jun N-terminal kinase (JNK; JNK-1 and -2) in glomeruli of rat PAN nephropathy. (Right) Effects of FR167653 administration on phospho-ERK levels in glomeruli of PAN nephropathy and ADR nephropathy on day 1. Magnification, ×400 in C and D; ×1000 in C and D inset.

Urinary Albumin Excretion in PAN and ADR Nephropathy

In rats with PAN nephropathy, no overt proteinuria was observed until day 4. Urinary albumin excretion showed a significant increase on day 7, peaked at approximately day 14, and returned to almost normal range by day 28 (Figure 3C). In mice with ADR nephropathy, urinary albumin excretion was normal until day 4, was significantly increased on day 7, reached to the peak level at approximately day 14, and remained significantly elevated through day 28 (Figure 3D). Such time courses were compatible with those in previous reports (6,7).

Effect of p38 MAPK Inhibitor on Proteinuria in PAN and ADR Nephropathy

Because the phosphorylation of p38 MAPK at podocytes preceded the onset of overt proteinuria, we hypothesized that the activation of p38 MAPK would critically be relevant to the appearance of proteinuria in these models of podocyte injury disease. We therefore investigated the effect of administration of FR167653, a specific inhibitor of p38 MAPK (15,16), to PAN and ADR nephropathy models on their renal outcomes. FR167653 has been reported to selectively inhibit p38α MAPK activity *in vitro*, without affecting the activities of other kinases,

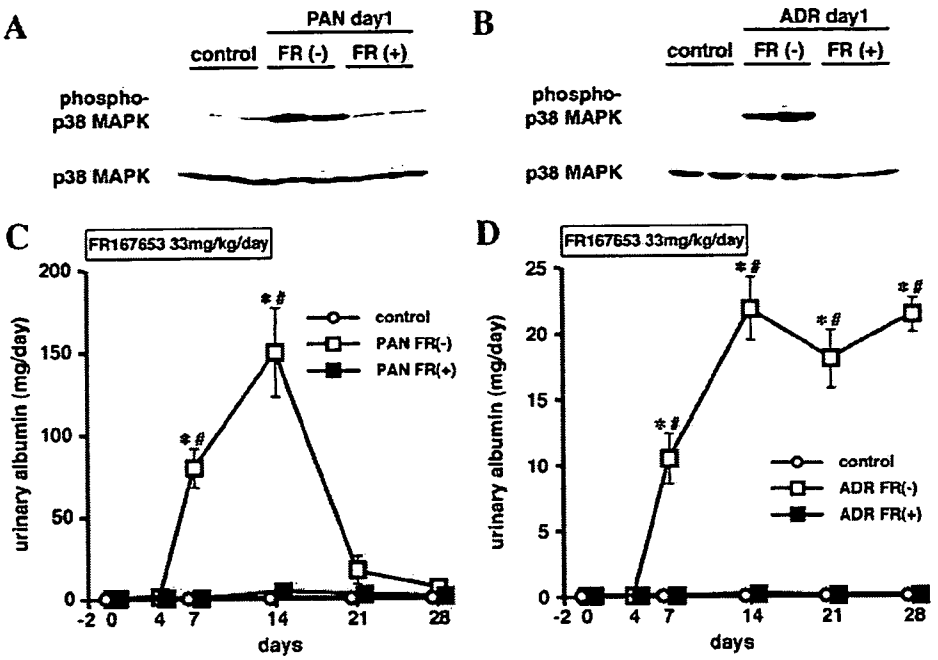

Figure 3. Effects of FR167653 administration on phospho–p38 MAPK levels in glomeruli and proteinuria in PAN nephropathy and ADR nephropathy. (A and B) Administration of FR167653 to animals with PAN nephropathy or ADR nephropathy abolished enhanced phosphorylation of p38 MAPK on day 1. (C and D) Urinary albumin excretion in nephrotic animals with or without FR167653. (C) In PAN nephropathy, urinary albumin increased on day 7, peaked at approximately day 14, and then decreased (□). Daily subcutaneous injection (day −2 to day 14) of FR167653 to rats with PAN nephropathy almost completely suppressed albumin excretion (■) to the control level (○). Mean ± SEM. $^*P < 0.05$ *versus* control; $^\#P < 0.05$ *versus* FR167653 treatment; $n = 7$. (D) In ADR nephropathy, urinary albumin increased on day 7, peaked at approximately day 14, and remained high through day 28 (□). Administration of FR167653 to mice with ADR nephropathy completely suppressed albumin excretion (■) to the control level (○). Mean ± SEM. $^*P < 0.05$ *versus* control; $^\#P < 0.05$ *versus* FR167653 treatment; $n = 7$.

including p38γ; ERK-1; JNK-2; protein kinases A, C, and G; and epidermal growth factor receptor (EGFR) kinase, as well as exerting no inhibitory effect on cyclooxygenase-1 or -2 activities, even at a dose 2 orders of magnitude higher than that for p38α MAPK inhibition (15).

In the glomeruli isolated from the animals that were pretreated with FR167653 from day −2, enhanced phosphorylation of p38 MAPK was effectively abolished to the control levels (Figure 3, A and B), indicating that the dose administered was sufficient to inhibit the activation of p38 MAPK at glomeruli *in vivo*. In this condition, we observed substantial inhibitory effects on the enhanced phosphorylation of ERK by administration of FR167653 in both models (Figure 2E, right), but the effects were less pronounced as compared with the effect on p38 MAPK; FR167653 did not affect JNK phosphorylation (data not shown). By daily subcutaneous administration of this compound to rats with PAN nephropathy for 17 d, urinary albumin excretion was almost completely suppressed to the control level (Figure 3C). Furthermore, in mice with ADR nephropathy, the administration of FR167653 for the same period completely abrogated the increase of urinary albumin excretion as well (Figure 3D). Thus, the blockade of p38 MAPK activation with FR167653 potently inhibited proteinuria in both models of podocyte injury disease, irrespective of initiating insults.

We next examined the effect of FR167653 administration after induction of the disease. When the compound was administered 4 h after induction of the diseases, FR167653 failed to suppress significantly the enhanced phosphorylation of p38 MAPK observed on day 1 (data not shown) in both models or subsequent increase in urinary albumin excretion (PAN day 14: 149.4 ± 26.8 *versus* 129.4 ± 18.8 mg/d; ADR day 14: 21.8 ± 2.6 *versus* 14.3 ± 2.1 mg/d; ADR day 28: 21.4 ± 1.5 *versus* 15.9 ± 3.8 mg/d; vehicle *versus* FR167653 treatment, respectively, $n = 4$). When the compound was injected 10 min after the induction of ADR nephropathy, half of the animals exhibited significant inhibition of phospho–p38 MAPK activation and effective suppression of the proteinuria near the control levels, but the rest showed almost no effect on p38 MAPK phosphorylation or proteinuria ($n = 3$ each).

Effect of p38 MAPK Inhibitor on Podocyte Injury

We next investigated the morphologic changes with or without inhibition of p38 MAPK. In electron microscopic analysis, the glomeruli with PAN nephropathy 2 wk after onset showed foot process effacement, with occasional vacuolation of podocytes (Figure 4A, middle). By contrast, glomeruli from FR167653-treated rats with PAN nephropathy revealed that foot processes were almost intact as in the control (Figure 4A). Likewise, glomeruli from mice with ADR nephropathy showed

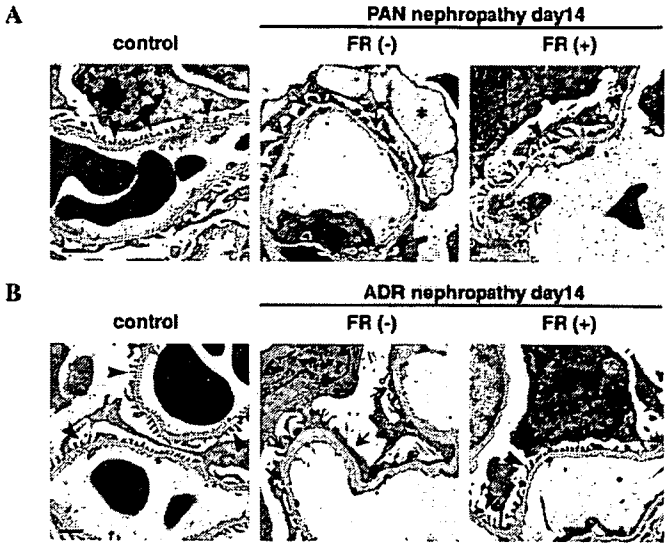

Figure 4. Electron microscopy of the glomerulus in podocyte injury models with or without FR167653. (A) Podocytes in control rats showed intact foot processes (arrowheads). PAN-treated rats on day 14 revealed foot process effacement (arrows), with occasional vacuolation of podocytes (*). In FR167653-administered rats with PAN nephropathy, most of the foot processes were intact [FR(+); arrowheads]. (B) Podocytes in control mice showed intact foot processes (arrowheads). Mice with ADR nephropathy on day 14 also showed foot process effacement (arrows), whereas FR167653 treatment retained normal foot processes [FR(+), arrowheads]. Bar = 1 μm.

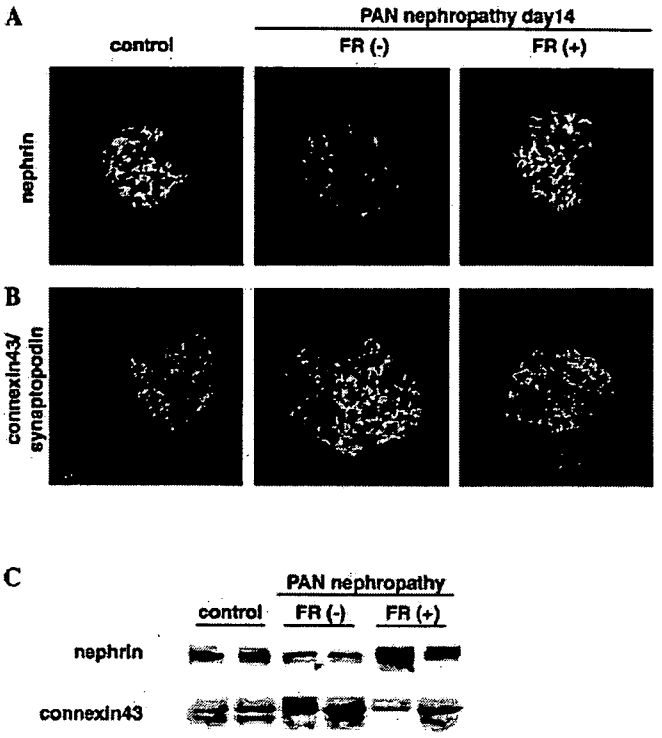

Figure 5. Expression of nephrin and connexin43 in PAN nephropathy with or without FR167653 on day 14. (A) Immunofluorescence study for nephrin. Normal glomerulus showed a linear staining pattern for nephrin along the capillary wall. PAN nephropathy revealed decreased intensity with a coarse granular pattern for nephrin. FR167653 treatment retained a normal linear pattern. (B) Immunofluorescence study for connexin43 (green) merged with synaptopodin (red). Podocytes in the control glomerulus rarely expressed connexin43. PAN nephropathy showed increased expression of connexin43 at podocytes. FR167653 treatment reduced its expression. (C) Western blotting for nephrin and connexin43 in glomeruli of PAN nephropathy with or without FR167653. Nephrin was decreased in PAN nephropathy, whereas FR167653 treatment showed no reduction in nephrin expression. By contrast, connexin43 was increased in PAN nephropathy, whereas FR167653 treatment decreased connexin43 expression to the control level.

marked foot process effacement, and the treatment with FR167653 prevented such changes (Figure 4B).

Nephrin, a product of the gene mutated in congenital nephrotic syndrome (22), is decreased and its distribution is altered upon proteinuric conditions in human nephrotic syndrome (23) and in animal models (8). We therefore investigated the expression and distribution pattern of nephrin in experimental animals. In Western blot and immunofluorescence analyses, rats with PAN nephropathy exhibited the decreased expression of nephrin on day 14, although FR167653-treated animals showed no reduction in nephrin expression (Figure 5, A and C). By immunofluorescence study, normal glomeruli showed a linear staining pattern for nephrin along the capillary wall, whereas glomeruli with PAN nephropathy exhibited a coarse granular staining pattern (Figure 5A). Rats that had PAN nephropathy and were treated with FR167653, however, retained such a linear pattern as seen in normal glomeruli (Figure 5A).

Connexin43 is a major gap junction protein that is expressed most abundantly among the connexin family in the kidney (24). Its expression is upregulated at podocytes upon injury (24) and therefore postulated as a marker for podocyte injury (19,24). We observed increased connexin43 in glomeruli with PAN nephropathy by Western blot and immunofluorescence analyses (Figure 5, B and C). By double-labeling immunofluorescence, glomerular expression of connexin43 in rats with PAN nephropathy merged with synaptopodin, a podocyte marker (21) (Figure 5B). FR167653 treatment in rats with PAN nephropathy reduced connexin43 expression at podocytes near the control level (Figure 5, B and C). Taken together, the administration of FR167653 in these rodent models of nephrotic syndrome prevented podocyte injury.

Effect of p38 MAPK Inhibitor on Glomerulosclerosis in ADR Nephropathy

By long-term follow-up of ADR nephropathy up to day 56, we observed persistent proteinuria (urinary albumin, 5.13 ± 1.49 mg/d; Figure 6A), together with chronic histologic changes such as tubular atrophy and focal glomerulosclerosis (Figure 6, B and C). The occurrence of sclerotic glomeruli out of total glomeruli per section showed a markedly higher rate in ADR nephropathy (Figure 6E). Some nonsclerotic glomeruli of

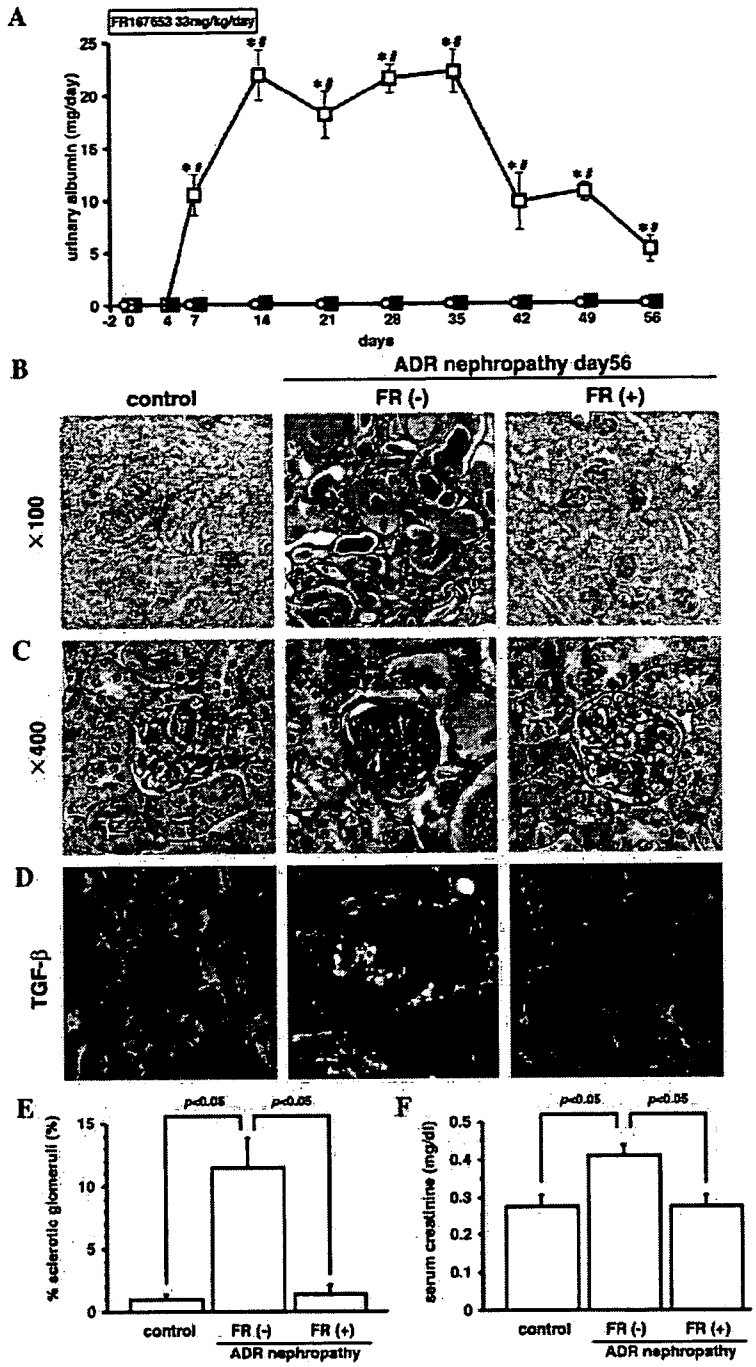

Figure 6. Effects of FR167653 administration on renal histology and function in mice with ADR nephropathy. (A) In ADR nephropathy, urinary albumin excretion persisted until day 56 (□). FR167653 treatment in these mice prevented overt albuminuria throughout the course (■), whose levels were similar to the control (○). Mean ± SEM. $^{*}P < 0.05$ *versus* control; $^{\#}P < 0.05$ *versus* FR167653 treatment; $n = 4$ to 7. (B) ADR nephropathy showed massive protein casts with marked tubular atrophy and degeneration. Administration of FR167653 revealed almost normal feature. (C) ADR nephropathy showed focal glomerulosclerosis, whereas FR167653 treatment revealed few sclerotic glomeruli. (D) Immunofluorescence study for TGF-β1. Some nonsclerotic glomeruli of ADR nephropathy exhibited an enhanced expression of TGF-β1, probably in the mesangial area. No glomeruli of FR167653-treated mice expressed TGF-β1. (E) The occurrence of sclerotic glomeruli on day 56 out of total glomeruli per section showed a markedly higher rate in ADR nephropathy than in control and FR167653 treatment. Mean ± SEM; $n = 4$. (F) The serum creatinine level on day 56 was significantly elevated in ADR nephropathy, but it remained normal with FR167653 treatment. Mean ± SEM; $n = 4$. Magnification, ×100 in B; ×400 in C, periodic acid-Schiff stain on day 56.

ADR nephropathy exhibited an enhanced glomerular expression of TGF-β1 (Figure 6D). Serum creatinine levels were also significantly elevated in ADR nephropathy (Figure 6F). Administration of FR167653 to mice with ADR nephropathy during the first 2 wk, however, maintained normal albumin excretion throughout the observation period (urinary albumin, 0.12 ± 0.07 mg/d on day 56; Figure 6A). Moreover, the treatment resulted in almost normal renal histology (Figure 6, B, C, and E), no glomerular augmentation of TGF-β1 (Figure 6D), and normal renal function (Figure 6F). Thus, FR167653 prevented the development of glomerulosclerosis and chronic renal dysfunction.

Effect of p38 MAPK Inhibitor on Actin Reorganization in Cultured Mouse Podocytes

Next we examined the effect of p38 MAPK activation on morphologic changes of podocytes using cultured mouse podocytes. Treatment of podocytes with PAN caused the phosphorylation of p38 MAPK (Figure 7A, left) and facilitated actin reorganization (Figure 7B). Pretreatment with FR167653 abolished the phosphorylation of p38 MAPK (Figure 7A) and prevented actin reorganization (Figure 7B). Likewise, the stimulation of podocytes with H_2O_2 as oxidative stress that activates p38 MAPK (10) increased phospho–p38 MAPK (Figure 7A, right) together with actin reorganization (Figure 7C). Pretreatment with FR167653 prevented these changes as well (Figure 7, A and C). Thus, the blockade of p38 MAPK activation inhibited actin reorganization.

Discussion

In this study, we investigated the significance of p38 MAPK in podocyte injury in clinical as well as experimental nephropathies and revealed that p38 MAPK activation at podocytes plays a crucial role for its pathophysiology. We showed an enhanced phosphorylation of p38 MAPK in glomeruli of clinical nephrotic syndrome. Furthermore, we demonstrated an essential role of p38 MAPK activation in rodent models of podocyte injury disease. In PAN nephropathy and ADR nephropathy, enhanced phosphorylation of p38 MAPK in the glomeruli was found during the first week of insult preceding overt proteinuria, and inhibition of p38 MAPK by FR167653

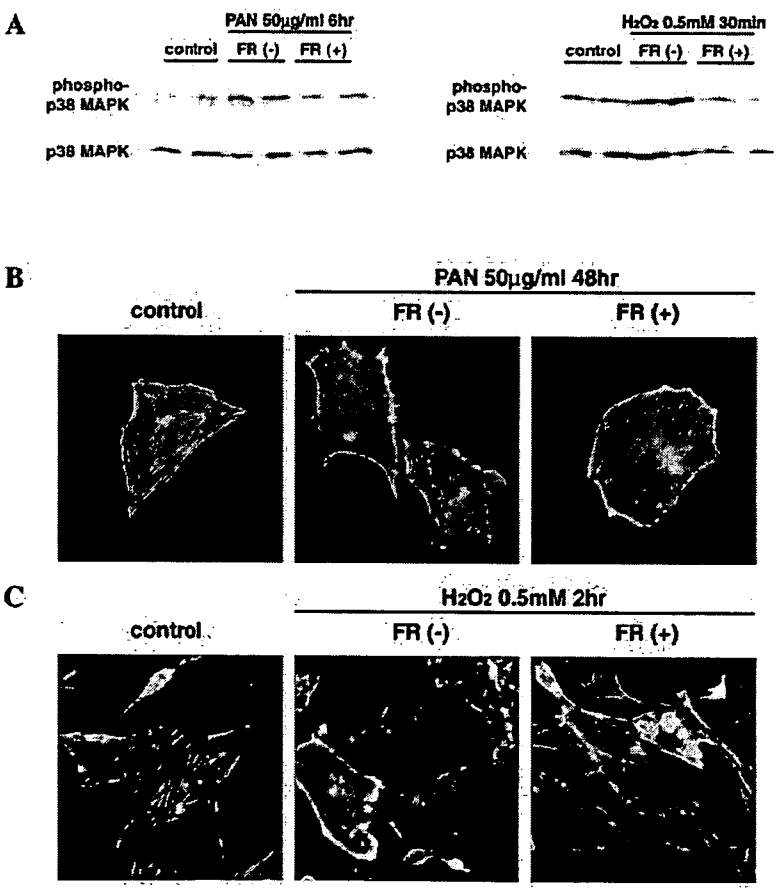

Figure 7. Effects of FR167653 on actin reorganization induced by PAN or oxidative stress. (A) In cultured podocytes, stimulation with PAN (50 μg/ml) for 6 h caused the phosphorylation of p38 MAPK. Pretreatment with FR167653 (10 μM) abolished p38 MAPK phosphorylation (left). Stimulation with H_2O_2 (0.5 mM) also increased phospho–p38 MAPK at 30 min, and pretreatment with FR167653 abrogated such increase (right). (B) Stimulation with PAN for 48 h caused actin reorganization in cultured podocytes, and pretreatment with FR167653 prevented actin reorganization. (C) Stimulation with H_2O_2 for 2 h also caused actin reorganization, which was prevented by FR167653 pretreatment.

resulted in marked suppression of podocyte injury and proteinuria. Moreover, the treatment with FR167653 during an early phase effectively prevented the progression of renal histologic changes in the chronic phase of ADR nephropathy. These findings strongly suggest that p38 MAPK activation should be functionally relevant to the pathogenesis of podocyte injury, serving as an upstream event necessary for proteinuria.

We observed an enhanced phosphorylation of p38 MAPK in human nephrotic states mainly in podocytes (Figure 1). It has already been reported that p38 MAPK activation in podocytes and tubules is found in various human nonproliferative as well as proliferative glomerulonephritis and correlates well with the degree of proteinuria and glomerular and/or interstitial injury (25). We also observed an enhanced p38 MAPK phosphorylation in podocytes of rodent models of nephrotic syndrome, especially during an early phase of the disease (Figure 2). It should be noted that there seems to be discrepancy between clinical nephropathies with sustained p38 MAPK phosphorylation and these rodent models with only transient activation of p38 MAPK. One explanation could be the difference in the cause and time course of podocyte injury. In experimental nephropathies, activation of p38 MAPK is elicited by a single burst of noxious stimulus, *i.e.*, injection of PAN or ADR, but in human glomerulopathies, p38 MAPK activation may be prolonged because of continuous stimuli such as circulating immune complexes. Although circumstantial, this might be reflected in different time courses of proteinuria between these models and clinical conditions. However, the pathogenic role for prolonged p38 MAPK activation in causing proteinuria and podocyte injury seen in clinical nephrotic syndrome should await further clarification.

In our study, there might be the time dissociation between p38 MAPK phosphorylation that occurred very early in these models and the appearance of overt proteinuria that occurred several days later (Figures 2 and 3). It is well conceivable that the activation of p38 MAPK in podocytes should trigger several intracellular signaling cascades, giving rise to serial reactions of the genes and proteins that alter cytoskeleton integrity or barrier function and finally lead to overt proteinuria. Proteinuria may ensue well behind (*e.g.*, months later) the transient activation and subsidence of triggering events, as shown in the ischemia/reperfusion injury model (26). In addition, a causal relationship between the only brief activation of p38 MAPK and the morphologic changes occurring several days later has been demonstrated in other cell types (27,28). Although the pretreatment by FR167653 in this study abrogated both the p38 MAPK activation and proteinuria, delayed FR167653 administration resulted in much less effect on proteinuria in parallel with the less efficient p38 MAPK inhibition (approximately 50% inhibition on both parameters when administered just after induction). These data may also suggest a close association between p38 MAPK activation and proteinuria.

Specificity of the inhibitor FR167653 for p38 MAPK is another issue to be addressed. Because this compound has been shown to selectively inhibit p38α MAPK without affecting ERK-1, JNK-2, or cyclooxygenase-1 and -2 *in vitro* (15), it is reasonable to assume that the results obtained here would be due to the specific inhibition of p38 MAPK (Figure 3A). The *in vivo* specificity of this compound, however, is not fully characterized. It is interesting that we found that FR167653 treatment attenuated ERK phosphorylation substantially, although not completely (Figure 2E), along with the complete inhibition of p38 MAPK activation. It is not clear at present whether such attenuation was direct and somehow contributed to the beneficial effects of this compound. Alternatively, ERK may have been downregulated secondary to p38 MAPK inhibition, as shown in thrombin-stimulated ERK activation in endothelium (29). Nevertheless, we cannot exclude the possibility that the beneficial effects of FR167653 exerted in this study could be due to either p38 MAPK or ERK pathway inhibition or both.

Activation of p38 MAPK is observed in embryonic kidneys and is required for renal development in rats (30). Although MAPK are thought to be largely inactive in adult kidneys at normal conditions, the activation of p38 MAPK can be detected in diseased kidneys from experimental models (16,31,32) and various human nephropathies (25,32,33). The role of p38 MAPK activation has been investigated so far by pharmacologic blockade in several experimental models. For example, p38 MAPK inhibition reduced proteinuria in anti-GBM glomerulonephritis (16) and ameliorated renal ischemia/reperfusion injury (34). In addition, blockade of p38 MAPK diminished angiotensin II–mediated renal damage, reducing mesangial matrix expansion (35). These reports have suggested that p38 MAPK should play important roles in cell proliferation or inflammatory responses in the mesangium and tubulointerstitium. In one report using complement-mediated cell injury, inhibition of p38 MAPK 7 d after induction of the disease failed to reverse and rather augmented cytotoxicity, suggesting that the activated p38 MAPK in podocytes may be cytoprotective during a later phase of this model (36). These studies, however, have not addressed the involvement of p38 MAPK in the pathogenesis of podocytopathies. In our study, we first demonstrate the pathogenic role of p38 MAPK activation in podocyte injury and proteinuria *in vivo* and effective prevention of the disease by an early inhibition of this activation. Furthermore, we reveal that the reduced expression of nephrin was effectively reversed by the treatment (Figure 5). Because nephrin expression largely correlates inversely with the degree of proteinuria (8,23), this perhaps may be an indirect consequence of inhibited proteinuria. Further study is needed to explore the relationship between nephrin expression and p38 MAPK activation.

In podocytes, several reports already investigated the role of p38 MAPK using conditionally immortalized mouse podocyte culture. p38 MAPK mediated TGF-β–induced apoptosis in podocytes (37). Because podocyte loss is a key event leading to glomerulosclerosis (38), p38 MAPK activation may facilitate glomerulosclerosis. High glucose exposure to podocytes stimulated p38 MAPK phosphorylation and α5(IV) collagen expression *via* the 12-lipoxygenase–dependent pathway (39). Furthermore, mechanical stretch induced the upregulation of cyclooxygenase-2 and prostaglandin EP4 receptor in a p38 MAPK–dependent manner (40), which may facilitate actin depolymerization (40). In addition, high glucose to podocytes stimulates the expression of vascular endothelial growth factor

(41), which in turn induces α3(IV) collagen production, acting downstream of TGF-β1 (42). Of note, in mesangial cells, vascular endothelial growth factor is induced by TGF-β1 *via* the p38 MAPK–dependent pathway and stimulates collagen and fibronectin expression (43). Whether such pathways are critically involved in the current beneficial effects exerted by p38 MAPK inhibition *in vivo* is not clear and requires further investigation.

How does p38 MAPK activation affect actin cytoskeleton and induce podocyte injury? By using cultured podocytes, we demonstrated a close association between p38 MAPK activation and actin reorganization induced by PAN or oxidative stress *in vitro*, and such changes were effectively abrogated by p38 MAPK inhibition (Figure 7). Therefore, one of the possibilities is that p38 MAPK activation may depolymerize actin filament through the molecule(s) that modulates actin polymerization. Several specific substrates for p38 MAPK that may be physiologically relevant have been identified. These include transcriptional factors ATF-2, CHOP, Elk-1, MEF2A, MEF2C, and Max, which can be phosphorylated and activated by p38 MAPK (10,44). p38 MAPK can also activate MAPK-activated protein kinases 2 and 3, which in turn phosphorylate small heat-shock protein 27 (hsp27) (10,13). Hsp27 is importantly involved in actin filament dynamics regulated by p38 MAPK (13), and the phosphorylated level of hsp27 is critically relevant to the morphologic changes and actin depolymerization in podocytes (45). Actin filament is a major constituent of foot processes, and depolymerization of actin filaments leads to foot process effacement (46). Because actin filaments interact with components of slit diaphragm and with integrins (46), depolymerized actin filaments may facilitate the loss of adhesive interactions, leading to disruption of slit diaphragm and detachment from GBM. Although p38 MAPK activation can induce actin reorganization *in vitro*, their molecular link is not demonstrated *in vivo*, and which molecular mechanisms are in fact involved in our study is unclear. Because the cell line of cultured podocytes used in this study does not form interdigitated foot processes or slit diaphragm (45), it will be required to establish the culture system reproducing the *in vivo* podocyte phenotypes to answer these questions.

Podocyte dysfunction leads to progressive renal insufficiency. First, podocyte damage causes proteinuria. Sustained proteinuria gives rise to tubulointerstitial injury, eventually leading to renal failure (47). Second, podocyte injury impairs mesangial structure and function. In anti–Thy-1 glomerulonephritis, a reversible self-limiting model in itself, preceding minor podocyte injury with PAN pretreatment results in irreversible mesangial alteration (48). We showed recently that cysteine-rich protein 61 (Cyr61), a potent angiogenic protein that belongs to the CCN family of matrix-associated secreted protein family, is expressed in podocytes and upregulated in anti–Thy-1 glomerulonephritis (20). Cyr61 inhibits mesangial cell migration, suggesting that Cyr61 may play a modulatory role in limiting mesangial activation (20). Thus, podocytes may secrete various humoral factors that regulate mesangial structure and function, and their reduction could result in impaired mesangial function such as mesangial proliferation and matrix expansion. Third, podocyte loss or detachment from the GBM leads to glomerulosclerosis (38). In human diabetic nephropathy and IgA nephropathy, decreased podocyte number correlates significantly with poor prognosis (49,50). These studies suggest that podocyte injury is critical not only in podocyte-specific diseases such as MCNS and FSGS but also in podocyte-nonspecific diseases such as IgA nephropathy.

In conclusion, our study reveals that the activation of p38 MAPK is crucial for podocyte injury in experimental nephrotic syndrome, suggesting that p38 MAPK activation is a common upstream mechanism necessary for podocyte injury in various proteinuric glomerulopathies. Although we need to be cautious in interpreting these results and extrapolating them to clinical situations, our study opens up a possibility that p38 MAPK and, possibly, ERK could become potential targets for therapeutic intervention in proteinuric glomerulopathies.

Acknowledgments

This work was supported in part by research grants from the Japanese Ministry of Education, Culture, Sports, Science and Technology; the Japanese Ministry of Health, Labor and Welfare; Smoking Research Foundation; and the Salt Science Research Foundation.

We gratefully acknowledge Dr. Peter Mundel (Albert Einstein College of Medicine, Bronx, NY) for the immortalized podocyte cell line, Dr. Sumio Kiyoto (Fujisawa Pharmaceutical, Osaka, Japan) for providing FR167653, and Drs. Shunji Nakatsuji and Yuji Oishi (Fujisawa Pharmaceutical) for electron microscopic analysis. We are also grateful to Junko Nakamura and Saori Saito for technical assistance and Shigeka Doi, Atsuko Sonoda, and Junichi Nomura for secretarial assistance.

References

1. Kriz W, Hackenthal E, Nobiling R, Sakai T, Elger M: A role for podocytes to counteract capillary wall distension. *Kidney Int* 45: 369–376, 1994
2. Drumond MC, Kristal B, Myers BD, Deen WM: Structural basis for reduced glomerular filtration capacity in nephrotic humans. *J Clin Invest* 94: 1187–1195, 1994
3. Laurens W, Battaglia C, Foglieni C, De Vos R, Malanchini B, Van Damme B, Vanrenterghem Y, Remuzzi G, Remuzzi A: Direct podocyte damage in the single nephron leads to albuminuria in vivo. *Kidney Int* 47: 1078–1086, 1995
4. Pavenstadt H: The charge for going by foot: Modifying the surface of podocytes. *Exp Nephrol* 6: 98–103, 1998
5. Barisoni L, Mundel P: Podocyte biology and the emerging understanding of podocyte diseases. *Am J Nephrol* 23: 353–360, 2003
6. Ryan GB, Karnovsky MJ: An ultrastructural study of the mechanisms of proteinuria in aminonucleoside nephrosis. *Kidney Int* 8: 219–232, 1975
7. Wang Y, Wang YP, Tay YC, Harris DC: Progressive adriamycin nephropathy in mice: Sequence of histologic and immunohistochemical events. *Kidney Int* 58: 1797–1804, 2000
8. Kawachi H, Koike H, Kurihara H, Yaoita E, Orikasa M, Shia MA, Sakai T, Yamamoto T, Salant DJ, Shimizu F: Cloning of rat nephrin: Expression in developing glomeruli and in proteinuric states. *Kidney Int* 57: 1949–1961, 2000
9. Kawachi H, Koike H, Kurihara H, Sakai T, Shimizu F: Cloning of rat homologue of podocin: Expression in pro-

teinuric states and in developing glomeruli. *J Am Soc Nephrol* 14: 46–56, 2003
10. Widmann C, Gibson S, Jarpe MB, Johnson GL: Mitogen-activated protein kinase: Conservation of a three-kinase module from yeast to human. *Physiol Rev* 79: 143–180, 1999
11. Adams JL, Badger AM, Kumar S, Lee JC: p38 MAP kinase: Molecular target for the inhibition of pro-inflammatory cytokines. *Prog Med Chem* 38: 1–60, 2001
12. Kimura C, Zhao QL, Kondo T, Amatsu M, Fujiwara Y: Mechanism of UV-induced apoptosis in human leukemia cells: Roles of Ca2+/Mg2+-dependent endonuclease, caspase-3, and stress-activated protein kinases. *Exp Cell Res* 239: 411–422, 1998
13. Guay J, Lambert H, Gingras-Breton G, Lavoie JN, Huot J, Landry J: Regulation of actin filament dynamics by p38 MAP kinase-mediated phosphorylation of heat shock protein 27. *J Cell Sci* 110: 357–368, 1997
14. Orikasa M, Matsui T, Oite T, Shimizu F: Massive proteinuria induced in rats by a single intravenous injection of a monoclonal antibody. *J Immunol* 141: 807–814, 1998
15. Takahashi S, Keto Y, Fujita T, Uchiyama T, Yamamoto A: FR167653, a p38 mitogen-activated protein kinase inhibitor, prevents *Helicobacter pylori*-induced gastritis in Mongolian gerbils. *J Pharmacol Exp Ther* 296: 48–56, 2001
16. Wada T, Furuichi K, Sakai N, Hisada Y, Kobayashi K, Mukaida N, Tomosugi N, Matsushima K, Yokoyama H: Involvement of p38 mitogen-activated protein kinase followed by chemokine expression in crescentic glomerulonephritis. *Am J Kidney Dis* 38: 1169–1177, 2001
17. Suganami T, Mukoyama M, Sugawara A, Mori K, Nagae T, Kasahara M, Yahata K, Makino H, Fujinaga Y, Ogawa Y, Tanaka I, Nakao K: Overexpression of brain natriuretic peptide in mice ameliorates immune-mediated renal injury. *J Am Soc Nephrol* 12: 2652–2663, 2001
18. Yokoi H, Mukoyama M, Nagae T, Mori K, Suganami T, Sawai K, Yoshioka T, Koshikawa M, Nishida T, Takigawa M, Sugawara A, Nakao K: Reduction in connective tissue growth factor by antisense treatment ameliorates renal tubulointerstitial fibrosis. *J Am Soc Nephrol* 15: 1140–1150, 2004
19. Suganami T, Mukoyama M, Mori K, Yokoi H, Koshikawa M, Sawai K, Hidaka S, Ebihara K, Tanaka T, Sugawara A, Kawachi H, Vinson C, Ogawa Y, Nakao K: Prevention and reversal of renal injury by leptin in a new mouse model of diabetic nephropathy. *FASEB J* 19: 127–129, 2005
20. Sawai K, Mori K, Mukoyama M, Sugawara A, Suganami T, Koshikawa M, Yahata K, Makino H, Nagae T, Fujinaga Y, Yokoi H, Yoshioka T, Yoshimoto A, Tanaka I, Nakao K: Angiogenic protein Cyr61 is expressed by podocytes in anti-Thy-1 glomerulonephritis. *J Am Soc Nephrol* 14: 1154–1163, 2003
21. Mundel P, Reiser J, Zuniga Mejia Borja A, Pavenstadt H, Davidson GR, Kriz W, Zeller R: Rearrangements of the cytoskeleton and cell contacts induce process formation during differentiation of conditionally immortalized mouse podocyte cell lines. *Exp Cell Res* 236: 248–258, 1997
22. Kestila M, Lenkkeri U, Mannikko M, Lamerdin J, McCready P, Putaala H, Ruotsalainen V, Morita T, Nissinen M, Herva R, Kashtan CE, Peltonen L, Holmberg C, Olsen A, Tryggvason K: Positionally cloned gene for a novel glomerular protein—nephrin—is mutated in congenital nephrotic syndrome. *Mol Cell* 1: 575–582, 1998
23. Furness PN, Hall LL, Shaw JA, Pringle JH: Glomerular expression of nephrin is decreased in acquired human nephrotic syndrome. *Nephrol Dial Transplant* 14: 1234–1237, 1999
24. Yaoita E, Yao J, Yoshida Y, Morioka T, Nameta M, Takata T, Kamiie J, Fujinaka H, Oite T, Yamamoto T: Up-regulation of connexin43 in glomerular podocytes in response to injury. *Am J Pathol* 161: 1597–1606, 2002
25. Stambe C, Nikolic-Paterson DJ, Hill PA, Dowling J, Atkins RC: p38 Mitogen-activated protein kinase activation and cell localization in human glomerulonephritis: Correlation with renal injury. *J Am Soc Nephrol* 15: 326–336, 2004
26. Takada M, Chandranker A, Nadeau KC, Sayegh MH, Tilney NL: The role of the B7 costimulatory pathway in experimental cold ischemia/reperfusion injury. *J Clin Invest* 100: 1199–1203, 1997
27. Morooka T, Nishida E: Requirement of p38 mitogen-activated protein kinase for neuronal differentiation in PC12 cells. *J Biol Chem* 273: 24285–24288, 1998
28. Galbiati F, Volonte D, Engelman JA, Scherer PE, Lisanti MP: Targeted down-regulation of caveolin-3 is sufficient to inhibit myotube formation in differentiating C2C12 myoblasts: Transient activation of p38 mitogen-activated protein kinase is required for induction of caveolin-3 expression and subsequent myotube formation. *J Biol Chem* 274: 30315–30321, 1999
29. Houliston RA, Pearson JD, Wheeler-Jones CPD: Agonist-specific cross talk between ERKs and p38 MAPK regulates PGI2 synthesis in endothelium. *Am J Physiol Cell Physiol* 281: C1266–C1276, 2001
30. Hida M, Omori S, Awazu M: ERK and p38 MAP kinase are required for rat renal development. *Kidney Int* 61: 1252–1262, 2002
31. Yin T, Sandhu G, Wolfgang CD, Burrier A, Webb RL, Rigel DF, Hai T, Whelan J: Tissue-specific pattern of stress kinase activation in ischemic/reperfused heart and kidney. *J Biol Chem* 272: 19943–19950, 1997
32. Adhikary L, Chow F, Nikolic-Paterson DJ, Stambe C, Dowling J, Atkins RC, Tesch GH: Abnormal p38 mitogen-activated protein kinase signalling in human and experimental diabetic nephropathy. *Diabetologia* 47: 1210–1222, 2004
33. Sakai N, Wada T, Furuichi K, Iwata Y, Yoshimoto K, Kitagawa K, Kokubo S, Kobayashi M, Takeda S, Kida H, Kobayashi K, Mukaida N, Matsushima K, Yokoyama H: p38 MAPK phosphorylation and NF-kappaB activation in human crescentic glomerulonephritis. *Nephrol Dial Transplant* 17: 998–1004, 2002
34. Furuichi K, Wada T, Iwata Y, Sakai N, Yoshimoto K, Kobayashi KK, Mukaida N, Matsushima K, Yokoyama H: Administration of FR167653, a new anti-inflammatory compound, prevents renal ischaemia/reperfusion injury in mice. *Nephrol Dial Transplant* 17: 399–407, 2002
35. de Borst MH, Navis G, de Boer RA, Huitema S, Vis LM, van Gilst WH, van Goor H: Specific MAP-kinase blockade protects against renal damage in homozygous TGR (mRen2)27 rats. *Lab Invest* 83: 1761–1770, 2003
36. Aoudjit L, Stanciu M, Li H, Lemay S, Takano T: p38 mitogen-activated protein kinase protects glomerular epithelial cells from complement-mediated cell injury. *Am J Physiol Renal Physiol* 285: F765–F774, 2003
37. Schiffer M, Bitzer M, Roberts IS, Kopp JB, ten Dijke P,

Mundel P, Bottinger EP: Apoptosis in podocytes induced by TGF-beta and Smad7. *J Clin Invest* 108: 807–816, 2001
38. Kriz W, Gretz N, Lemley KV: Progression of glomerular diseases: Is the podocyte the culprit? *Kidney Int* 54: 687–697, 1998
39. Kang SW, Natarajan R, Shahed A, Nast CC, Mundel P, Kashtan C, Adler SG: Role of 12-lipoxygenase in the stimulation of p38 mitogen-activated protein kinase and collagen alpha5(IV) in experimental diabetic nephropathy and in glucose-stimulated podocytes. *J Am Soc Nephrol* 14: 3178–3187, 2003
40. Martineau LC, McVeigh LI, Jasmin BJ, Kennedy CRJ: p38 MAP kinase mediates mechanically induced COX-2 and PG EP4 receptor expression in podocytes: Implications for the actin cytoskeleton. *Am J Physiol Renal Physiol* 286: F693–F701, 2004
41. Iglesias-de la Cruz MC, Ziyadeh FN, Isono M, Kouahou M, Han DC, Kalluri R, Mundel P, Chen S: Effects of high glucose and TGF-beta1 on the expression of collagen IV and vascular endothelial growth factor in mouse podocytes. *Kidney Int* 62: 901–913, 2002
42. Chen S, Kasama Y, Lee JS, Jim B, Martin M, Ziyadeh FN: Podocyte-derived vascular endothelial growth factor mediates the stimulation of alpha3(IV) collagen production by transforming growth factor-beta1 in mouse podocytes. *Diabetes* 53: 2939–2949, 2004
43. Wang L, Kwak JH, Kim SI, He Y, Choi ME: Transforming growth factor-beta1 stimulates vascular endothelial growth factor 164 via mitogen-activated protein kinase kinase 3-p38alpha and p38delta mitogen-activated protein kinase-dependent pathway in murine mesangial cells. *J Biol Chem* 279: 33213–33219, 2004
44. Zhu T, Lobie PE: Janus kinase 2-dependent activation of p38 mitogen-activated protein kinase by growth hormone: Resultant transcriptional activation of ATF-2 and CHOP, cytoskeletal re-organization and mitogenesis. *J Biol Chem* 275: 2103–2114, 2000
45. Smoyer WE, Ransom RF: Hsp27 regulates podocyte cytoskeletal changes in an in vitro model of podocyte process retraction. *FASEB J* 16: 315–326, 2002
46. Mundel P, Shankland SJ: Podocyte biology and response to injury. *J Am Soc Nephrol* 13: 3005–3015, 2002
47. Remuzzi G, Bertani T: Pathophysiology of progressive nephropathies. *N Engl J Med* 339: 1448–1456, 1998
48. Morioka Y, Koike H, Ikezumi Y, Ito Y, Oyanagi A, Gejyo F, Shimizu F, Kawachi H: Podocyte injuries exacerbate mesangial proliferative glomerulonephritis. *Kidney Int* 60: 2192–2204, 2001
49. Pagtalunan ME, Miller PL, Jumping-Eagle S, Nelson RG, Myers BD, Rennke HG, Coplon NS, Sun L, Meyer TW: Podocyte loss and progressive glomerular injury in type II diabetes. *J Clin Invest* 99: 342–348, 1997
50. Lemley KV, Lafayette RA, Safai M, Derby G, Blouch K, Squarer A, Myers BD: Podocytopenia and disease severity in IgA nephropathy. *Kidney Int* 61: 1475–1485, 2002

THE JOURNAL OF BIOLOGICAL CHEMISTRY
Vol. 280, No. 15, Issue of April 15, pp. 15247–15256, 2005
Printed in U.S.A.

Analysis of Rat Insulin II Promoter-Ghrelin Transgenic Mice and Rat Glucagon Promoter-Ghrelin Transgenic Mice*

Received for publication, October 5, 2004, and in revised form, February 3, 2005
Published, JBC Papers in Press, February 8, 2005, DOI 10.1074/jbc.M411358200

Hiroshi Iwakura‡, Kiminori Hosoda‡§, Choel Son‡, Junji Fujikura‡, Tsutomu Tomita‡, Michio Noguchi‡, Hiroyuki Ariyasu‡, Kazuhiko Takaya‡‖, Hiroaki Masuzaki‡, Yoshihiro Ogawa‡, Tatsuya Hayashi‡, Gen Inoue‡, Takashi Akamizu‖, Hiroshi Hosoda‖, Masayasu Kojima‡‡, Hiroshi Itoh‡, Shinya Toyokuni¶, Kenji Kangawa‖**, and Kazuwa Nakao‡**

*From the ‡Department of Medicine and Clinical Science, Endocrinology and Metabolism and ¶Department of Pathology and Biology of Diseases, Kyoto University Graduate School of Medicine, 54 Shogoin Kawahara-cho, Sakyo-ku, Kyoto 606-8507, the ‖Translational Research Center, Kyoto University Hospital, Kyoto 606-8507, the ‡‡Department of Molecular Genetics, Institute of Life Science, Kurume University, Fukuoka 839-0861, and the **Department of Biochemistry, National Cardiovascular Center Research Institute, Osaka 565-8565, Japan*

We developed and analyzed two types of transgenic mice: rat insulin II promoter-ghrelin transgenic (RIP-G Tg) and rat glucagon promoter-ghrelin transgenic mice (RGP-G Tg). The pancreatic tissue ghrelin concentration measured by C-terminal radioimmunoassay (RIA) and plasma desacyl ghrelin concentration of RIP-G Tg were about 1000 and 3.4 times higher than those of nontransgenic littermates, respectively. The pancreatic tissue *n*-octanoylated ghrelin concentration measured by N-terminal RIA and plasma *n*-octanoylated ghrelin concentration of RIP-G Tg were not distinguishable from those of nontransgenic littermates. RIP-G Tg showed suppression of glucose-stimulated insulin secretion. Arginine-stimulated insulin secretion, pancreatic insulin mRNA and peptide levels, β cell mass, islet architecture, and GLUT2 and PDX-1 immunoreactivity in RIP-G Tg pancreas were not significantly different from those of nontransgenic littermates. Islet batch incubation study did not show suppression of insulin secretion of RIP-G Tg *in vitro*. The insulin tolerance test showed lower tendency of blood glucose levels in RIP-G Tg. Taking lower tendency of triglyceride level of RIP-G Tg into consideration, these results may indicate that the suppression of insulin secretion is likely due to the effect of desacyl ghrelin on insulin sensitivity. RGP-G Tg, in which the pancreatic tissue ghrelin concentration measured by C-RIA was about 50 times higher than that of nontransgenic littermates, showed no significant changes in insulin secretion, glucose metabolism, islet mass, and islet architecture. The present study raises the possibility that desacyl ghrelin may have influence on glucose metabolism.

Ghrelin is a 28-amino acid peptide with unique modification of acylation, which is essential for its biological action (1). Ghrelin was originally identified in rat stomach as an endogenous ligand for an orphan receptor, which has been so far called growth hormone secretagogue receptor (GHS-R)[1] (1). Ghrelin expression is detected in the stomach, intestine, hypothalamus, pituitary gland, kidney, placenta, and testis (2–6). Ghrelin is involved in a wide variety of the functions, including the regulation of growth hormone release, food intake, gastric acid secretion, gastric motility, blood pressure, and cardiac output (7–19).

Recently Date *et al.* (20) reported that ghrelin is present in α cells of normal human and rat pancreatic islets. Volante *et al.* (21) described ghrelin-expression in β cells of human islet. Wierup *et al.* and Prado *et al.* reported that ghrelin-expressing cells are a new islet cell type distinct from α, β, δ, and PP cells in human, rat, and mouse islets (22–24). Although there was no apparent change of plasma insulin levels in ghrelin null mouse (25, 26), which may indicate that ghrelin is not a direct regulator of insulin secretion in the physiological condition, there have been several reports of the effect of pharmacological dose of ghrelin on insulin secretion. Broglio *et al.*, Egido *et al.*, and Reimer *et al.* have reported that ghrelin has an inhibitory effect on insulin secretion (27–30). Adeghate *et al.*, Date *et al.*, and Lee *et al.* have reported that ghrelin stimulates insulin secretion (20, 31, 32). Salehi *et al.* have reported ghrelin has both inhibitory and stimulatory effects depending on its concentration (33). Therefore, there is still a lot of controversy about the localization of ghrelin in the pancreas and the effects of ghrelin on the insulin secretion. As for the effects of desacyl ghrelin on insulin secretion, Broglio *et al.* (34) have reported that acute desacyl ghrelin administration has no effect on insulin secretion in human but that it counteracts the inhibitory effect of *n*-octanoylated ghrelin on insulin secretion when co-administrated with *n*-octanoylated ghrelin (35).

Here we developed and analyzed two types of transgenic mice: rat insulin II promoter-ghrelin transgenic mice (RIP-G Tg) and rat glucagon promoter-ghrelin transgenic mice (RGP-G Tg). The purpose of this study was to clarify the effect of transgenic overexpression of ghrelin cDNA in pancreatic islets.

EXPERIMENTAL PROCEDURES

Generating RIP- and RGP-ghrelin Transgenic Mice—Mouse stomach cDNA library was constructed from 1 μg of mouse stomach poly(A)$^+$

* This work was supported by research grants from the Japanese Ministry of Education, Culture, Sports, Science and Technology, the Japanese Ministry of Health, Labor and Welfare. The costs of publication of this article were defrayed in part by the payment of page charges. This article must therefore be hereby marked "*advertisement*" in accordance with 18 U.S.C. Section 1734 solely to indicate this fact.

§ To whom correspondence should be addressed. Tel.: 81-75-751-3172; Fax: 81-75-771-9452; E-mail: kh@kuhp.kyoto-u.ac.jp.

[1] The abbreviations used are: GHS-R, growth hormone secretagogue receptor; RIP-G Tg, rat insulin II promoter-ghrelin transgenic; RGP-G Tg, rat glucagon promoter-ghrelin transgenic mice; RIA, radioimmunoassay; C-RIA, anti-ghrelin [13–28] antiserum; N-RIA, anti-ghrelin [1–11] antiserum; RT, reverse transcription; HDL, high density lipoprotein; PP, pancreatic polypeptide.

RNA with a cDNA synthesis kit (Amersham Biosciences). Mouse ghrelin cDNA was isolated from this library, using rat ghrelin cDNA as a probe. A fusion gene comprising RIP and mouse ghrelin cDNA coding sequences was designed. The purified fragment (10 μg/ml) was microinjected into the pronucleus of fertilized C57/B6J mice (SLC, Shizuoka, Japan) eggs. The viable eggs were transferred into the oviducts of pseudopregnant female ICR mice (SLC) using standard techniques. Transgenic founder mice were identified by Southern blot analysis of tail DNAs using the mouse ghrelin cDNA fragment as a probe. RGP-G Tg was generated similarly. Transgenic mice were used as heterozygotes. Animals were maintained on standard rat food (CE-2, 352 kcal/100 g, Japan CLEA, Tokyo, Japan) on a 12-h light/12-h dark cycle. All experimental procedures were approved by the Kyoto University Graduate School of Medicine Committee on Animal Research.

Immunohistochemistry—Formalin-fixed, paraffin-embedded tissue sections were immunostained using the avidin-biotin peroxidase complex method (Vectastain "ABC" Elite kit, Vector Laboratories, Burlingame, CA) as described previously (36). Serial sections were used, and the thickness of each section was 5 μm. Sections were incubated with anti-C-terminal ghrelin [13–28] (1:1000 at final dilution), anti-N-terminal ghrelin [1–11] (1:2000) (1), which recognizes the *n*-octanoylated portion of ghrelin, anti-glucagon (1:500), anti-insulin (1:500), anti-somatostatin (1:500), anti-pancreatic polypeptide (PP, 1:500, DAKO, Glostrup, Denmark), anti-PDX-1 (1:2000, kindly provided by Christopher V. E. Wright) (37), and anti-GLUT2 (1:200, kindly provided by Bernard Thorens) (38) antisera. Quantification of β cell area was performed in insulin-stained sections by using Axio Vision (Carl Zeiss, Hallbergmoos, Germany) and Scion Image (Scion Corp., Frederick, MD). Ten sections (200-μm interval) for each mouse ($n = 5$) were analyzed. The percentage of β cell area in the pancreas was determined by dividing the area of all insulin-positive cells in one section by the total area of the section.

Measurements of Plasma and Tissue Ghrelin Concentrations—Plasma was sampled from 10-week-old RIP-G Tg and their nontransgenic littermates under ad libitum feeding states considering the promoter activity. From RGP-G Tg and their littermates, it was sampled after overnight fast. Blood was withdrawn from the retroorbital vein or the proximal end of the portal vein under ether anesthesia, immediately transferred to chilled siliconized glass tubes containing Na_2EDTA (1 mg/ml) and aprotinin (1000 KIU/ml, Ohkura Pharmaceutical, Kyoto, Japan), and centrifuged at 4 °C. Hydrogen chloride was added to the samples at a final concentration of 0.1 N immediately after separation of plasma. Plasma was immediately frozen and stored at −80 °C until assay. Plasma ghrelin concentration was determined by desacyl ghrelin enzyme-linked immunosorbent assay kit and active-ghrelin enzyme-linked immunosorbent assay kit that recognizes *n*-octanoylated ghrelin (Mitsubishi Kagaku Iatron, Tokyo, Japan).

As for measurement of tissue ghrelin concentration, pancreata or stomachs were taken from the 8-week-old male mice. The rumen was removed from the stomach. Samples were diced and boiled for 5 min in the 10-fold v/w of water. Acetic acid was added to each solution so that the final concentration was adjusted to 1 M, and the tissues were homogenized. The supernatants were obtained after centrifugation. Tissue ghrelin concentration was determined by radioimmunoassay (RIA) using anti-ghrelin [13–28] antiserum (C-RIA) and anti-ghrelin [1–11] antiserum (N-RIA) as described previously (39).

Measurements of Body Weight and Food Consumption—Mice were housed individually and were allowed free access to standard rat chow. Body weights of mice were measured weekly. Daily food intake was measured by weighing the pellets between 9:00 and 10:00 a.m.

Measurements of % Body Fat and Visceral/Subcutaneous Fat Mass Ratio—Forty-week-old mice were anesthetized with pentobarbital. Percent body fat and visceral/subcutaneous fat mass ratio of mice were measured by Latheta LTC-100 (ALOKA, Tokyo, Japan).

Glucose and Insulin Tolerance Tests—For the glucose tolerance test, after overnight fast, the mice were injected with 1.5 g/kg glucose intraperitoneally. For the insulin tolerance test, after a 4-h fast, mice were injected with 2.0 milliunits/g human regular insulin (Novolin R; Novo Nordisk, Bagsvaerd, Denmark) intraperitoneally. Blood was sampled from the tail vein before and 15, 30, 60, 90, and 120 min after the injection. Blood glucose levels were determined by glucose oxidase method using Glutest sensor (Sanwa Kagaku, Kyoto, Japan).

Insulin Release—After overnight fast, the mice were injected with 3.0 g/kg glucose or 0.25 g/kg L-arginine intraperitoneally. Plasma was sampled from the tail vein before and 2, 5, 15, 30, and 60 min after the injection using heparin coated tubes. The measurement of insulin concentration was carried out by enzyme-linked immunosorbent assay using ultra-sensitive rat insulin kit (Morinaga, Yokohama, Japan).

Pancreatic Insulin Concentration—As for measurement of pancreatic insulin concentration, pancreata were obtained from the mice under the ether anesthesia and homogenized in acid-ethanol. The supernatants were used for assay after centrifugation.

Batch Incubation of Islet—Under the pentobarbital anesthesia, Type IV collagenase (Worthington, Lakewood, NJ) dissolved in Hanks' balanced salt solution (1.5 mg/ml) was injected into mouse pancreatic duct. Pancreas was removed and incubated at 37 °C for 14 min. After washing out collagenase by Hanks' balanced salt solution, islets were collected by Ficoll gradient and manually picked up so that the sizes of the islets were equal. Islets were incubated at 37 °C in RPMI1640 containing 10% fetal calf serum for 2 h and then in Krebs-Ringer bicarbonate buffer containing 3.3 mM glucose and 0.2% bovine serum albumin for 30 min. Five islets were incubated at 37 °C in 500 μl of Krebs-Ringer bicarbonate buffer containing 0.2% bovine serum albumin and 3.3 or 8.7 or 16.7 mM glucose for 1 h. After centrifugation, the supernatants were collected. Insulin concentrations in supernatants were determined by rat insulin kit (Morinaga, Yokohama, Japan).

Northern Blot Analysis and Real-time Quantitative RT-PCR—Total RNA was extracted from pancreata using RNeasy mini kit (Qiagen K.K., Tokyo, Japan). Filters containing 5 μg of total RNA were prepared. Northern blot analyses were performed as described previously (36) using the mouse insulin II cDNA and human β-actin cDNA (Clontech, Palo Alto, CA) as probes. To confirm that approximately equal amounts of total RNA were assayed in Northern blot hybridization analysis, the density of 18 S rRNA in the gel and signal of β-actin in each lane was used. The hybridization signal intensity was quantitated using an image analyzer BAS-2500 (Fuji Photo Film, Tokyo, Japan). Reverse transcription (RT) was performed with random hexamer and SuperScript II reverse transcriptase (Invitrogen). Real-time quantitative PCR was performed with ABI PRISM 7700 Sequence Detection System (Applied Biosystems, Foster City, CA). The following primers and TaqMan probes were used: mouse GHS-R (sense, 5′-CACCAACCTCTACCTATCCAGCAT-3′; antisense, 5′-CTGACAAACTGGAAGAGTTTGCA-3′; TaqMan probe, 5′-TCCGATCTGCTCATCTTCCTGTGCATG-3′); mouse ghrelin (sense, 5′-GCATGCTCTGGATGGACATG-3′; antisense, 5′-TGGTGGCTTCTTGGATTCCT-3′; TaqMan probe, 5′-AGCCCAGAGCACCAGAAAGCCCA-3′).

Lipid Measurements—Blood was collected from the retroorbital vein of 35-week-old RIP-G Tg and their nontransgenic littermates. After separation of serum, total cholesterol, triglyceride, free fatty acid, and HDL-cholesterol levels in serum were determined by Cholesterol E-test Wako, Triglyceride E-test Wako, NEFA C-test Wako, and HDL-cholesterol E-test Wako (Wako Pure Chemical Industries, Osaka, Japan).

Statistical Analysis—All values were expressed as means ± S.E. Statistical significance of difference in mean values was assessed by repeated measures analysis of variance or Student's *t* test.

RESULTS

Distribution of Ghrelin in Normal Mouse Pancreas—We first examined which cell type of islet cells expresses ghrelin in mouse by immunohistochemistry using anti-C-terminal ghrelin antiserum. In the most of the islets no ghrelin-like immunoreactivity was detected. C-terminal ghrelin-like immunoreactivity was observed in the periphery of minor proportion of islets of wild type mice (Fig. 1*A*). Most of the ghrelin-positive cells were also glucagon-positive by serial section analysis (Fig. 1*B*), whereas most of the glucagon-positive cells were not ghrelin-positive.

Generation of RIP- and RGP-ghrelin Transgenic Mice—A fusion gene comprising RIP and mouse ghrelin cDNA coding sequences was designed so that ghrelin expression might be targeted to the pancreatic β cells (Fig. 2*A*). The ghrelin mRNA level of RIP-G Tg in pancreas determined by quantitative RT-PCR was about 215 times higher than that of nontransgenic littermates (215.3 ± 40.6 *versus* 1.0 ± 0.025 arbitrary units, $n = 5$, $p < 0.01$). There was also an increase in ghrelin mRNA levels in brain of RIP-G Tg (242.6 ± 17.6 *versus* 89.1 ± 27.3 arbitrary unit, $n = 5$, $p < 0.01$). To confirm the expression of ghrelin transgene in pancreatic β cells, we performed an immunohistochemical analysis using anti-C-terminal ghrelin antiserum. C-terminal ghrelin-like immunoreactivity was observed in the nearly whole area of the islets of the RIP-G Tg (Fig. 2*C*), whereas it was only seen in the periphery of the islets

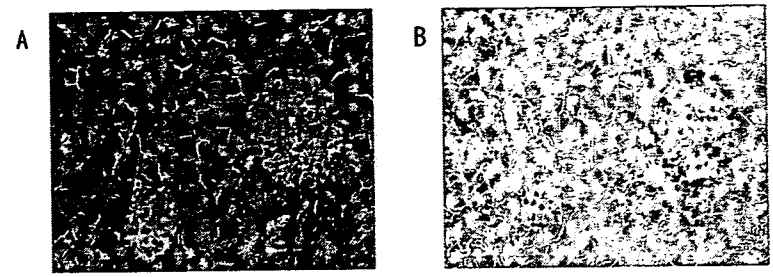

FIG. 1. *A*, C-terminal ghrelin-like immunoreactivity in adult mouse islet. The staining was observed in the peripheral region of the islet. *B*, glucagon-like immunoreactivity in serial section.

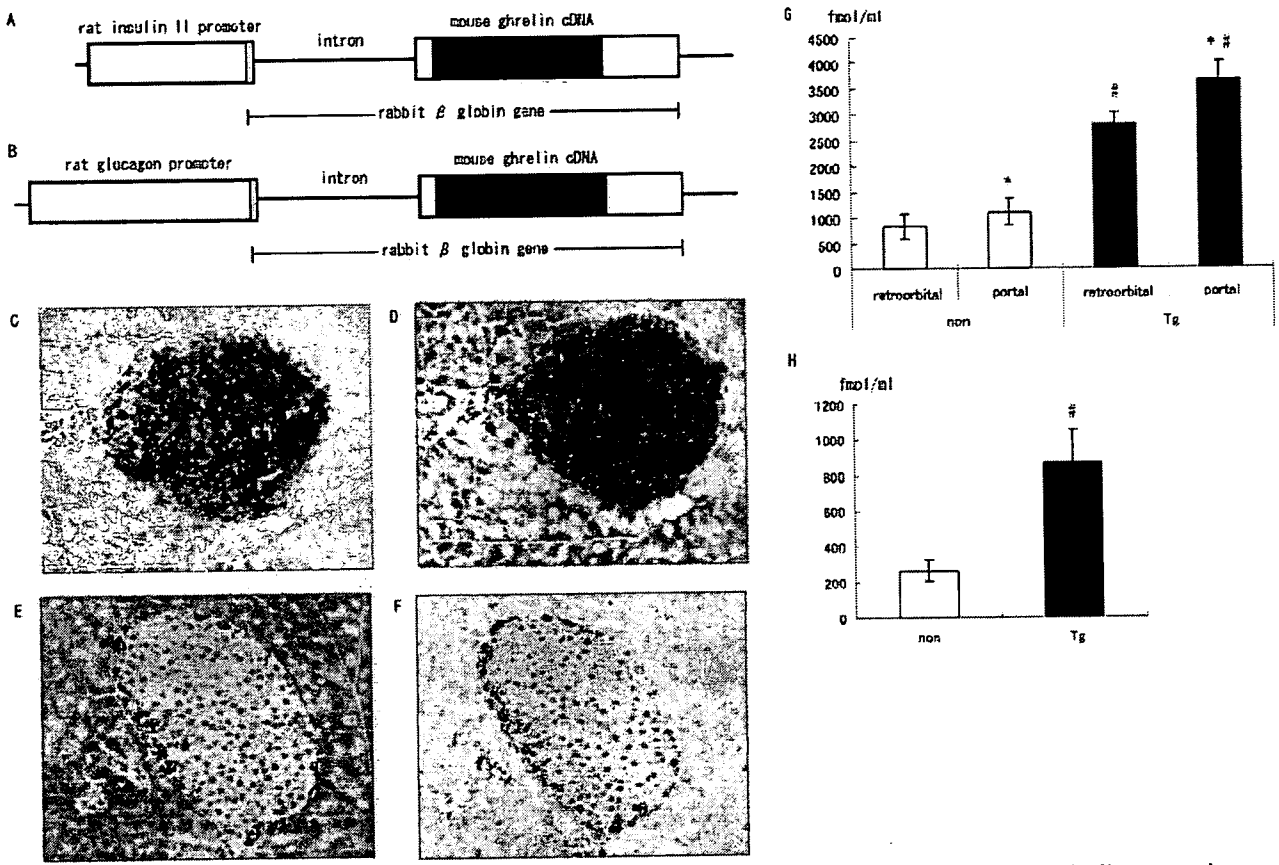

FIG. 2. *A*, structure of RIP-ghrelin transgene. *B*, structure of RGP-ghrelin transgene. *C* and *D*, pancreatic islet of RIP-ghrelin transgenic mouse stained with anti-C-terminal ghrelin (*C*) and anti-N-terminal ghrelin antisera (*D*). *E* and *F*, pancreatic islet of RGP-ghrelin transgenic mouse stained with anti-C-terminal ghrelin (*E*) and anti-N-terminal ghrelin antisera (*F*). *G*, plasma ghrelin levels collected from retroorbital and portal veins in RIP-G Tg. *, $p < 0.05$ compared with retroorbital vein. #, $p < 0.01$ compared with nontransgenic littermates. *H*, the step-up of ghrelin concentration from retroorbital vein to portal vein in RIP-G Tg. #, $p < 0.01$ compared with their nontransgenic littermates.

of their nontransgenic littermates (Fig. 1*A*). Immunohistochemical analysis using anti-N-terminal ghrelin antiserum showed the same staining pattern (Fig. 2*D*), indicating that *n*-octanoylated ghrelin may be produced in β cells of this transgenic mouse. We also stained the brain section of RIP-G Tg. No ghrelin-like immunoreactivity was detected either with anti-C-terminal or anti-N-terminal ghrelin antisera (data not shown). The pancreatic tissue ghrelin concentration of RIP-G Tg measured by C-RIA was about 1000 times higher than that of their nontransgenic littermates (1024 ± 108.9 fmol/mg *versus* 1.2 ± 0.1 fmol/mg, $n = 5$, $p < 0.01$). This concentration was about one third of the nontransgenic stomach concentration (3558.1 ± 51.0 fmol/mg, $n = 5$). The pancreatic tissue ghrelin concentration of RIP-G Tg measured by N-RIA tended to be also higher than that of their nontransgenic littermates (0.054 ± 0.017 fmol/mg *versus* 0.038 ± 0.006fmol/mg, $n = 5$, NS; not significant), but it did not reach statistical significance. Plasma desacyl ghrelin concentration of RIP-G Tg was about 3.4 times higher than that of nontransgenic littermates under the ad libitum feeding states (2805.5 ± 236.4 *versus* 825.9 ± 244.4 fmol/ml, $n = 5$, $p < 0.01$, Fig. 2*G*). We also measured desacyl ghrelin levels in portal vein of the mice. In the nontransgenic mice, the portal desacyl ghrelin level was significantly higher than that in retroorbital vein (1108.0 ± 257.3 fmol/ml *versus* 825.9 ± 244.4 fmol/ml, $n = 5$, $p < 0.05$, Fig. 2*G*). The desacyl ghrelin concentration collected from portal vein of RIP-G Tg at the same time was much higher than that of nontransgenic littermates (3671.8 ± 328.6 *versus* 1108.0 ± 257.3 fmol/ml, $n = 5$, $p < 0.01$, Fig. 2*G*). The step-up of desacyl ghrelin concentration from retroorbital vein to portal vein of RIP-G Tg was significantly higher than that of nontransgenic littermates (866.3 ± 182.2 fmol/ml *versus* 262.9 ± 59.8 fmol/ml, $p < 0.01$, Fig. 2*H*). Plasma *n*-octanoylated ghrelin levels in retroorbital and portal vein of RIP-G Tg tended to be higher than those of their nontransgenic littermates (retroorbital: 78.5 ± 13.4 *versus* 66.1 ± 7.1 fmol/ml, $n = 5$, NS; portal: 104.6 ± 15.3 *versus*

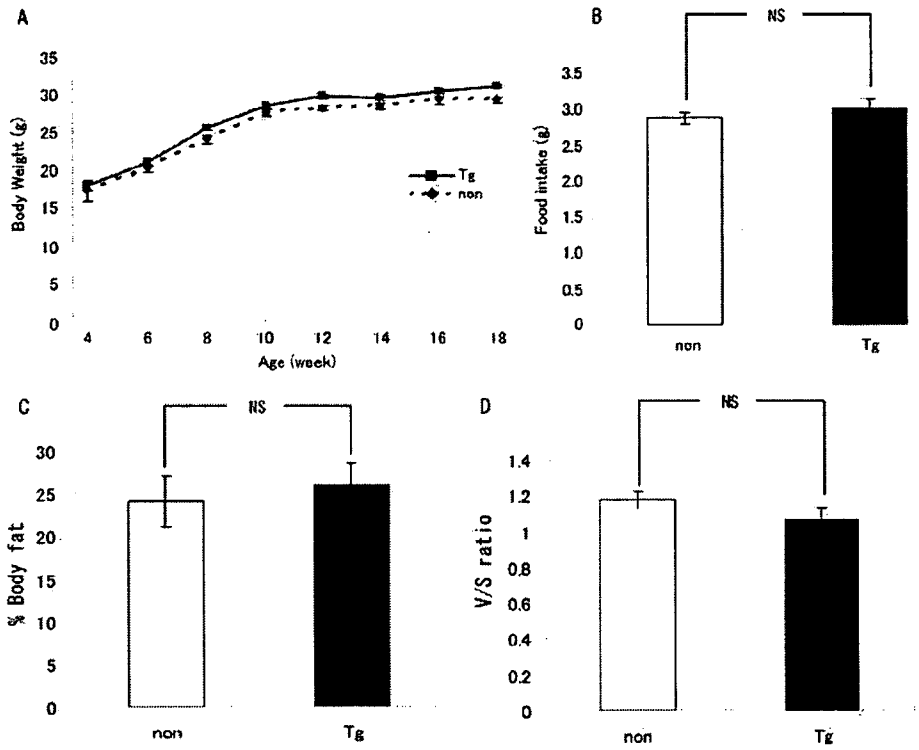

FIG. 3. *A*, body weight of RIP-G Tg (*Tg*) and their nontransgenic littermates (*non*). *B*, food intake of RIP-GTg (*Tg*) and their nontransgenic littermates (*non*). Percent body fat (*C*) and visceral/subcutaneous fat ratio (*D*) of RIP-GT$_g$ and their nontransgenic littermates (*non*).

71.4 ± 9.0 fmol/ml, n = 5, NS), but it did not reach statistical significance.

We also generated RGP-G Tg, in which ghrelin expression is targeted to the pancreatic α cells (Fig. 2*B*). The ghrelin mRNA level Tg in pancreas of RGP-G determined by quantitative RT-PCR was about 16 times higher than that of nontransgenic littermates (16.3 ± 1.7 *versus* 1.0 ± 0.24 arbitrary unit, n = 5, $p < 0.01$). The ghrelin mRNA level in duodenum of RGP Tg was not statistically different from that of nontransgenic littermates (520.1 ± 111.1 *versus* 379.1 ± 37.6 arbitrary unit, n = 5, NS). The ghrelin mRNA level in brain of RGP Tg was not distinguishable from that of nontransgenic littermates (72.0 ± 6.4 *versus* 71.8 ± 7.8 arbitrary unit, n = 5, NS). Immunohistochemical analysis showed ghrelin-like immunoreactivity in the periphery of the pancreatic islet of RGP-ghrelin transgenic mouse by both anti-C-terminal ghrelin and anti-N-terminal ghrelin antisera (Fig. 2, *E* and *F*). The pancreatic tissue ghrelin concentrations of RGP-G Tg measured by C-RIA were about 50 times higher than those of their nontransgenic littermates (48.9 ± 2.5 fmol/mg *versus* 1.2 ± 0.1 fmol/mg, n = 5, $p < 0.01$). The pancreatic tissue ghrelin concentration of RGP-G Tg measured by N-RIA tended to be higher than that of their nontransgenic littermates (0.076 ± 0.019 fmol/mg *versus* 0.038 ± 0.006 fmol/mg, n = 5, NS), but it did not reach statistical significance. The plasma desacyl ghrelin concentrations in retroorbital vein were not elevated in RGP-G Tg after over night fasting compared with nontransgenic littermates (661.6 ± 38.0 *versus* 1024.7 ± 27.1 fmol/ml, n = 5). The portal desacyl ghrelin concentrations of RGP-G Tg were also indistinguishable from those of their nontransgenic littermate (1320.6 ± 164.7 *versus* 1442.9 ± 361.5 fmol/ml, n = 5, NS). Plasma n-octanoylated ghrelin levels in retroorbital and portal vein of RGP-G Tg were indistinguishable from those of their nontransgenic littermates (retroorbital: 98.3 ± 18.7 *versus* 133.5 ± 25.3 fmol/ml, n = 5, NS; portal: 154.3 ± 20.7 *versus* 198.9 ± 34.9 fmol/ml, n = 5, NS).

Body Weight, Food Consumption, and Percent Body Fat—There was no significant difference in body weight and food intake between RIP-G Tg and their nontransgenic littermates (Fig. 3). Percent body fat and visceral/subcutaneous ratio of RIP-G Tg were not different from those of nontransgenic littermates (Fig. 2, *C* and *D*). No significant changes were observed in RGP-G Tg, either (data not shown).

Glucose Metabolism and Insulin Secretion—Although no significant differences in blood glucose levels were noted between RIP-G Tg and their nontransgenic littermates on the fasting state and intraperitoneal glucose tolerance tests (Fig. 4, *A* and *C*), plasma insulin levels 2 and 30 min after the glucose injection were significantly decreased in RIP-G Tg compared with those in their nontransgenic littermates (Fig. 4*D*). Suppression of insulin secretion was not observed in RIP-G Tg on intraperitoneal injection of arginine (Fig. 4*G*). Blood glucose level of RIP-G Tg in the insulin tolerance test tended to be lower than those of their nontransgenic littermates, but it did not reach statistical significance (Fig. 4*H*).

No significant differences in blood glucose or insulin levels were observed between RGP-G Tg and their nontransgenic littermates on the fasting state, ad libitum feeding, or intraperitoneal glucose or arginine injection (Fig. 4, *B*, *E*, and *F*, and data not shown). Blood glucose levels on insulin tolerance test showed no differences between RGP-ghrelin and their nontransgenic littermates (data not shown).

Islet Architecture and β Cell Mass—We studied the tissue sections of RIP-G Tg to explore the effect of ghrelin on the islet architecture and β cell mass. There were no obvious abnormalities in the intra islet cytoarchitecture and cell number of insulin, glucagon, somatostatin, and PP cells in the islets of the RIP-G Tg (Fig. 5*A–D*). The intensity of staining of these four islet hormones in the islets of the RIP-G Tg was not apparently different from those of nontransgenic littermates. The ratio of the β cell area to whole pancreas was not changed significantly

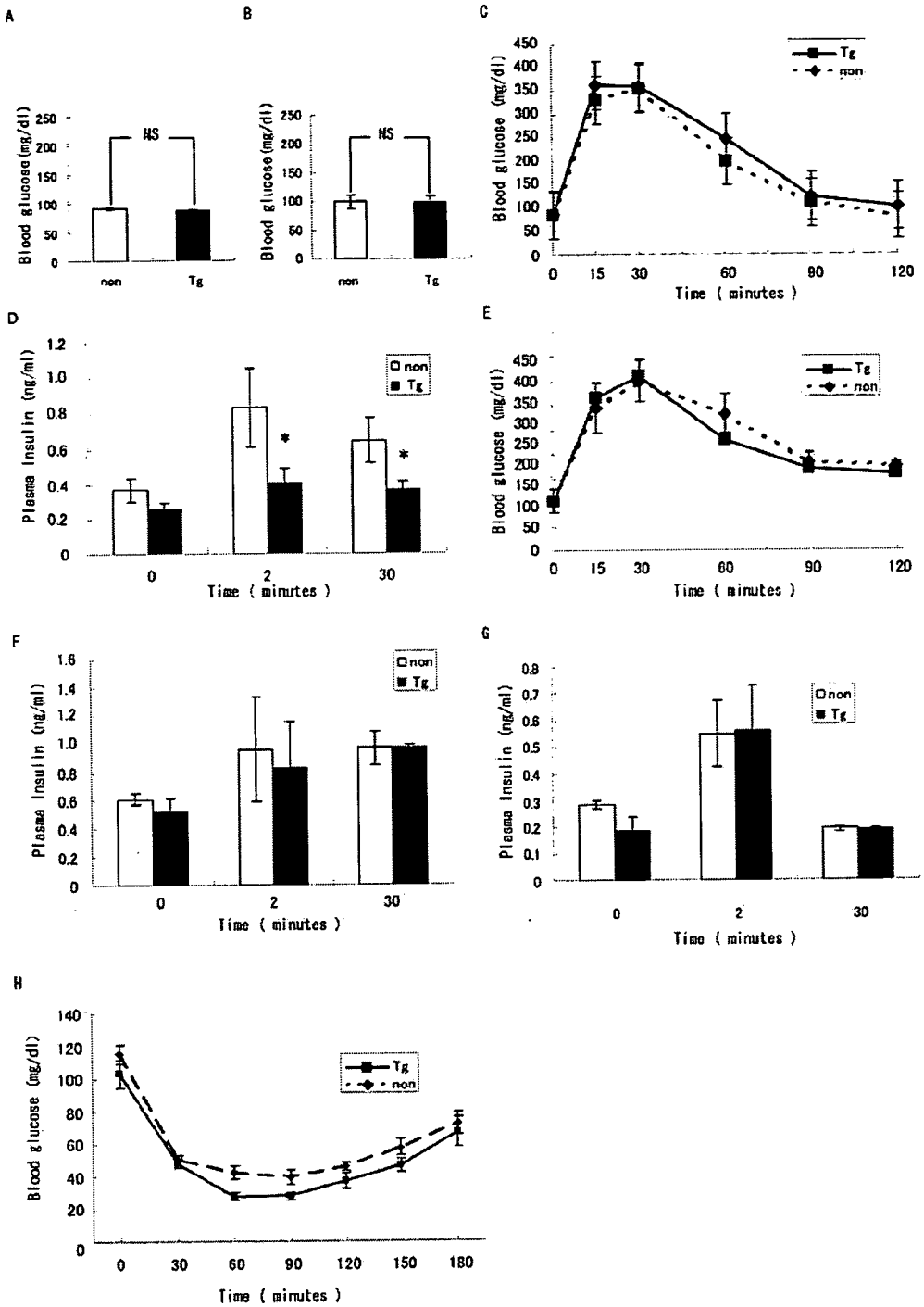

FIG. 4. *A* and *B*, blood glucose levels after overnight fast in RIP-G Tg (*A*) and RGP-G Tg (*B*) (*Tg*) and their nontransgenic littermates (*non*). *C* and *E*, intraperitoneal (*IP*) glucose tolerance test (1.5 g/kg) in RIP-G Tg (*C*) and RGP-G Tg (*E*) (*Tg*) and their nontransgenic littermates (*non*). *D* and *F*, plasma insulin concentration after intraperitoneal glucose (3g/kg) injection in RIP-G Tg (*D*) and RGP-G Tg (*F*) (*Tg*) and their nontransgenic littermates (*non*). *G*, plasma insulin concentration after intraperitoneal arginine (0.25g/kg) injection in RIP-G Tg (*Tg*) and their nontransgenic littermates (*non*). *H*, insulin (2.0 units/kg) tolerance test in RIP-G Tg (*Tg*) and their nontransgenic littermates (*non*). Values are represented as mean ± S.E. *, $p < 0.05$ compared with nontransgenic littermates.

(Fig. 5*I*). We also studied the tissue sections of RGP-G Tg and found no significant differences (Fig. 5, *E–H*, and *J*).

Expression of Insulin mRNA and Insulin Content—Because RIP-G Tg showed suppression of insulin secretion, we examined pancreatic mRNA expression and peptide content of insulin in RIP-G Tg and their nontransgenic littermates by Northern blot analysis and RIA. The insulin mRNA in RIP-G Tg did not differ from those of their nontransgenic littermates (Fig. 6, *A* and *B*). No significant differences of insulin contents were observed between RIP-G Tg and their nontransgenic littermates (Fig. 6*C*).

PDX-1 and GLUT2 Immunoreactivity—We examined the immunoreactivity of PDX-1 and GLUT2 in RIP-G Tg. The staining intensities of PDX-1 and GLUT2 in the RIP-G Tg (Fig. 7, *A*

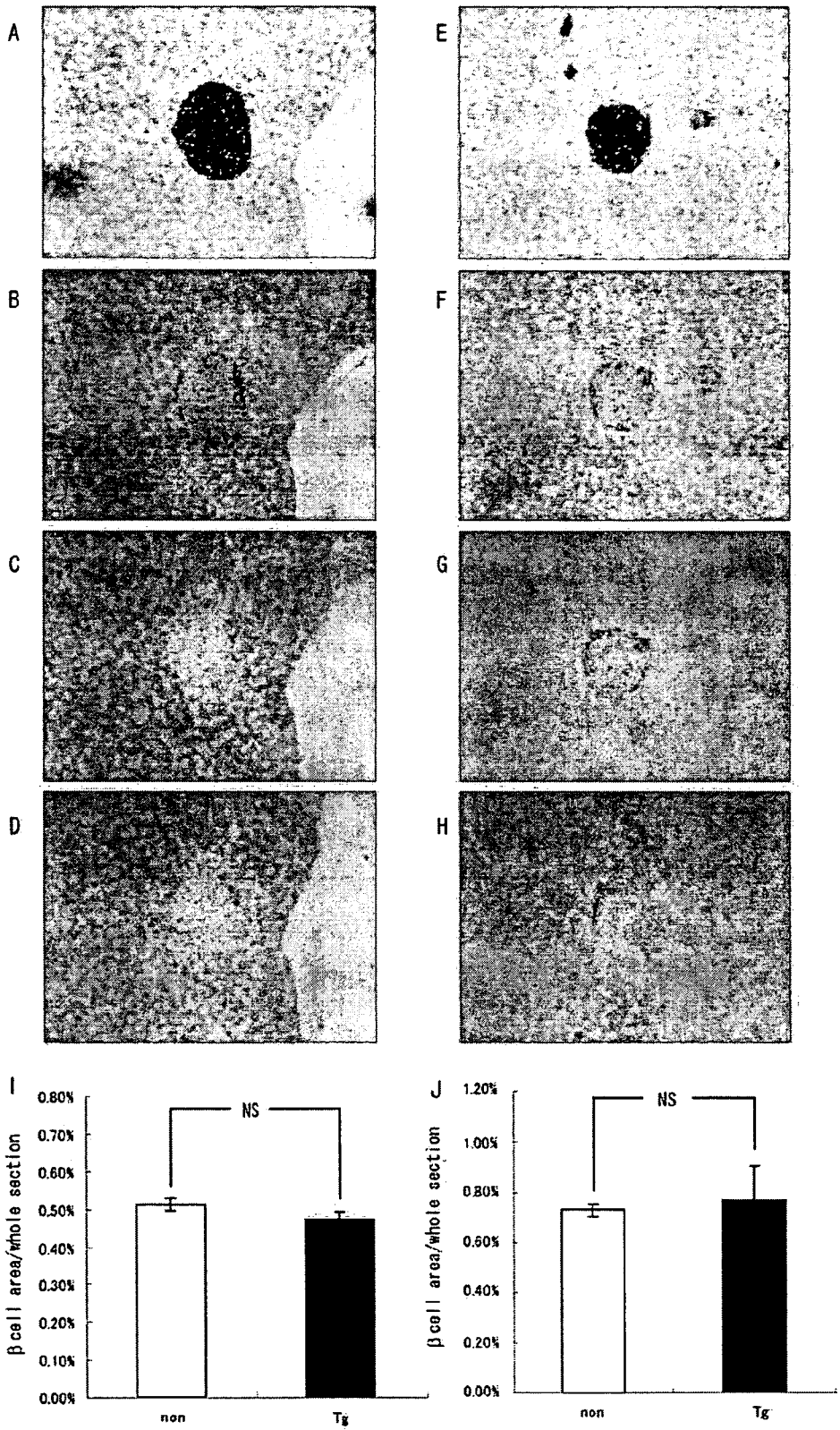

FIG. 5. **Islet morphology and β cell area in RIP-G Tg (*A–D*) and RGP-G Tg (*E–H*).** The sections were stained with anti-insulin (*A* and *E*), anti-glucagon (*B* and *F*), anti-somatostatin (*C* and *G*), and anti-PP antiserum (*D* and *H*). *I* and *J*, the ratio of β cell area to that of whole section in RIP-G Tg (*I*) and RGP-G Tg (*J*). *non*, nontransgenic littermates; *Tg*, RIP-G Tg; *NS*, not significant.

and *C*) were not apparently different from those in the nontransgenic littermates (Fig. 7, *B* and *D*).

Expression of GHS-R mRNA—To rule out possible down-regulation of GHS-R due to chronic exposure to high level ghrelin, we measured the expression level of GHS-R mRNA in pancreas and pituitary by real-time quantitative RT-PCR.

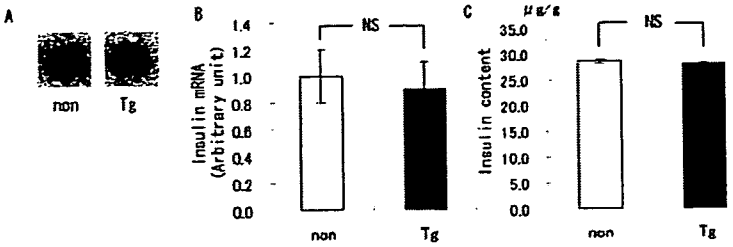

FIG. 6. **mRNA level and peptide content of insulin in RIP-G Tg (*Tg*) and their nontransgenic littermates (*non*) pancreas.** *A*, representative blot of Northern blot analysis of insulin; *B*, insulin mRNA levels; *C*, insulin peptide contents. *NS*, not significant.

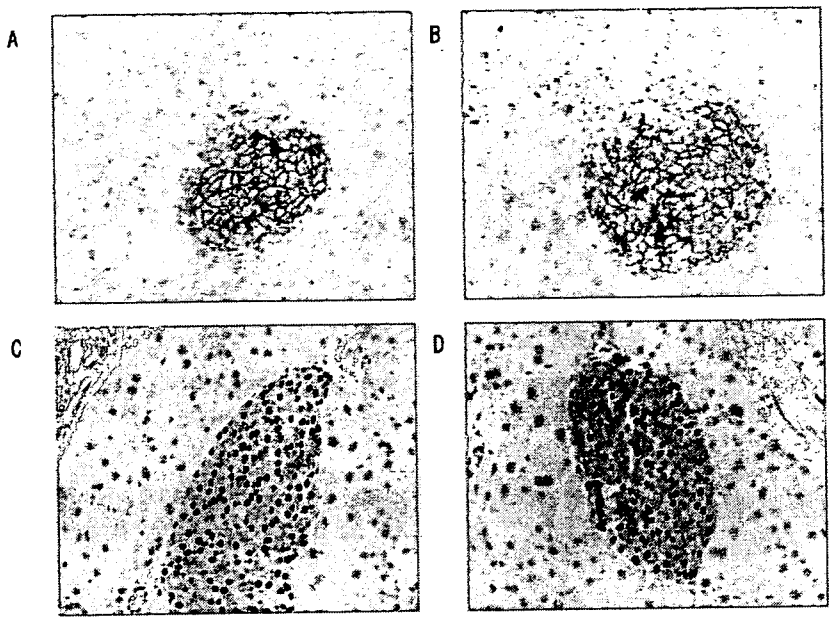

FIG. 7. *A* and *B*, immunoreactivity of Glut-2 in the islet of RIP-G Tg (*A*) and nontransgenic littermates (*B*). *C* and *D*, immunoreactivity of PDX-1 in the islet of RIP-G Tg (*C*) and nontransgenic littermates (*D*).

There were no significant differences in GHS-R mRNA levels between RIP-G Tg and their nontransgenic littermates either in pancreas (Fig. 8*A*) or in pituitary (Fig. 8*B*).

Batch Incubation of Islets—The insulin secretion from isolated islet of RIP-G Tg by batch incubation was indistinguishable from that of nontransgenic littermates, in 3.3 or 8.7 or 16.7 mM glucose conditions (Fig. 9).

Lipid Metabolism—Plasma total cholesterol level of RIP-G Tg tended to be lower than those of nontransgenic littermates, but it did not reach statistical significance (total cholesterol: 85.4 ± 6.9 *versus* 79.4 ± 7.5 mg/dl, n = 6, NS). The plasma triglyceride level of RIP-G Tg tended to be lower than that of nontransgenic littermates, but it did not reach statistical significance (154.5 ± 11.0 *versus* 136.9 ± 10.3 mg/dl, n = 6, NS). Free fatty acid level and HDL-cholesterol level of RIP-G Tg were not significantly different from those of nontransgenic littermates (free fatty acid; 0.44 ± 0.05 *versus* 0.48 ± 0.07 mEq/liter, n = 6, NS, HDL-cholesterol; 46.1 ± 2.3 *versus* 44.9 ± 3.4 mg/dl, n = 6, NS).

DISCUSSION

In wild-type mice, no ghrelin-like immunoreactivity was detected in most of the islets. C-terminal ghrelin-like immunoreactivity was observed in the periphery of minor proportion of islets of wild type mice, which is consistent with a previous report (24). By the serial section analysis, most of the ghrelin-producing cells also showed glucagon-like immunoreactivity. These findings indicate that ghrelin was expressed in minor proportion of mouse pancreatic α cells. Expression of ghrelin was not detected in pancreatic β cells of wild type mice.

In the present study we developed RIP-G Tg, in which pancreatic ghrelin concentration measured by C-RIA was ~1000 times higher than that of nontransgenic littermates. By immunohistochemistry using anti-C-terminal ghrelin [13–28] antiserum we detected C-terminal ghrelin-like immunoreactivity in almost the whole area of islets. Therefore, because ghrelin was not detected in β cells of control mice by immunohistochemistry, ghrelin transgene driven by RIP was considered to be expressed in β cells.

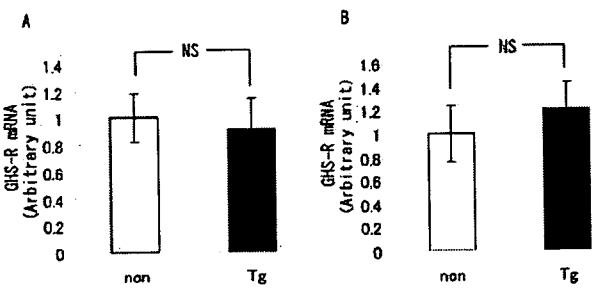

FIG. 8. **mRNA level of GHS-R determined by quantitative RT-PCR in pancreas (*A*) and pituitary (*B*) of RIP-G Tg (*Tg*) and their nontransgenic littermates (*non*).** *NS*, not significant.

We also found about 3 times higher expression level of ghrelin mRNA in the brain of RIP-G Tg compared with that of nontransgenic littermates, which could not be detected by immunohistochemistry. Although a small amount of ghrelin has been reported to be expressed in brain, which can be detected by immunohistochemistry only after colchicine treatment (1), there have been controversies as to whether this small amount of ghrelin in the brain has a biological role. Because the food intake of RIP-G Tg was not different from that of nontransgenic littermates, the ghrelin produced by transgene in the brain seems not to show bioactive effect of n-octanoylated ghrelin.

By immunohistochemistry using anti-ghrelin [1–11] anti-

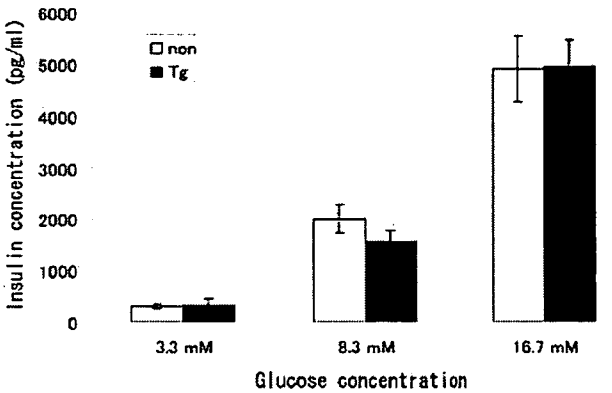

FIG. 9. **Batch incubation study of isolated islets of RIP-G Tg (*Tg*) and their nontransgenic littermates (*non*).**

serum that recognizes the *n*-octanoylated portion of ghrelin, ghrelin-like immunoreactivity was also demonstrated in nearly whole area of islets of RIP-G Tg, indicating the production of *n*-octanoylated ghrelin in β cells. This finding indicates that the mechanism of acylation may exist not only in pancreatic α cells but also in β cells. This is reasonable, because α and β cells are pancreatic endocrine cells derived from common precursor cells (40). Because the N-RIA/C-RIA ratio of the pancreatic tissue ghrelin concentration of RIP-G Tg was much lower than that of the stomach (0.0053% *versus* 11.67%, $p < 0.01$), the ability of acylation in β cell might be lower than that of in ghrelin-producing cell in the stomach (X/A-like cell). It is possible that exocrine pancreatic enzymes might interfere with the results, although these were inactivated by boiling before extraction. The other possibility is that because of the formalin fixation of ghrelin in the tissue section the epitope recognized by immunohistochemistry using anti-ghrelin [1–11] antiserum might not be exactly the same as that recognized by N-RIA or enzyme-linked immunosorbent assay. Because the amount of *n*-octanoylated ghrelin was so little that it could not be detected by RIA if any, we considered that the phenotype of these transgenic mice is due to the effect of desacyl ghrelin. Desacyl ghrelin has been shown not to activate GHS-R (39). There have been several reports saying that desacyl ghrelin has biological activities, such as promoting adipogenesis (41), inhibition of cell proliferation, inhibition of apoptosis (42), and counteracting the effect of *n*-octanoylated ghrelin (35).

We showed here that the ghrelin level in portal vein is significantly higher than that in retroorbital vein in wild type mouse. Ghrelin has been reported to be mainly synthesized in stomach and intestine. The step-up of plasma ghrelin level in gastric vein has been reported previously (43), but there has been no report showing the step-up of plasma ghrelin level in portal vein as compared with that in systemic circulation. The present study is the first report of the step-up of plasma ghrelin levels in portal vein. Moreover, the step-up of desacyl ghrelin in RIP-G Tg was much higher than that in control littermates, indicating overproduction of desacyl ghrelin by transgene in the pancreas.

The body weight, percent body fat, and food consumption of RIP-G Tg were not significantly different from those of nontransgenic littermates. Recently, we and Asakawa *et al.* have reported the studies of β-actin promoter ghrelin transgenic mouse (44, 45), in which plasma desacyl ghrelin levels were 30 and 50 times higher than those of their nontransgenic littermates. These transgenic mice were reported to show small phenotype, although some discrepancy of interpretation regarding on etiology exists. Asakawa *et al.* reported that the triglyceride level of β-actin promoter ghrelin transgenic mouse was lower, but that cholesterol level and free fatty acid level were not changed compared with their nontransgenic littermates. The triglyceride levels of our RIP-G Tg only showed lower tendency compared with that of nontransgenic littermates. The lack of small phenotype and milder phenotype of lipid metabolism in RIP-G Tg may result from the fact that plasma desacyl ghrelin level of RIP-G Tg was only 3.4 times higher than those of nontransgenic littermates.

The tissue sections of the pancreas of these transgenic mice showed no apparent disarrangement in the islet architecture and in β cell mass. There have been several reports on the transgenic mice overexpressing humoral factors in the β cells, such as parathyroid hormone-related peptide, hepatocyte growth factor, and insulin-like growth factor-I (46–49). Some of these transgenic mice showed islet hypertrophy or disarrangement of the endocrine cells in the islet (46–49). Our observation showed that desacyl ghrelin might have no apparent effects on the islet architecture and β cell mass.

In the present study plasma insulin levels after the 3.0 g/kg glucose injection were significantly lower in RIP-G Tg than those in nontransgenic littermates, although there was no significant difference in plasma insulin levels between RIP-G Tg and nontransgenic littermates on the fasting state. To rule out the decreased production of insulin caused by exogenous insulin promoter, we measured insulin mRNA level and content in the pancreata of our transgenic mice. The insulin mRNA level and content from the transgenic mice were not significantly different from those from nontransgenic littermates. Therefore, the insulin production might not be disturbed in these mice either in transcriptional or translational levels. The immunoreactivity of PDX-1, which is the master regulator of the pancreas development and essential for insulin transcription, in RIP-G Tg β cell was not different from that in β cells of nontransgenic littermates. These results suggest that the suppression of glucose-stimulated insulin secretion in RIP-G Tg might not be due to the transcriptional dysregulation of insulin caused by injection of exogenous insulin promoter.

RIP-G Tg did not show decreased-insulin secretion in response to arginine. Arginine is known to stimulate insulin secretion by the mechanisms that are different from those used by glucose, although the detail remains controversial (50, 51). However, it seems certain that arginine somehow evoked Ca^{2+} influx into the β cell, and that leads to the exocytosis of insulin-containing vesicles (52, 53). So at least, the decreased insulin secretion in RIP-G Tg might not be due to disorders in exocytosis process. Egido (28) reported that ghrelin inhibits insulin secretion from rat pancreas in response to arginine *in vitro*, however, there has been no report on the effect of desacyl ghrelin on arginine-induced insulin secretion.

The immunoreactivity of GLUT2, glucose transporter in the pancreatic β cell, in RIP-G Tg β cells, was indistinguishable from that in the β cells of nontransgenic littermates. Although immunohistochemistry is not so suitable for quantitative analysis, at least no apparent decreased expression or disposition of GLUT2 in RIP-G Tg β cell exists. Chronic exposure to the high level of desacyl ghrelin may not influence on GLUT2 expression.

We performed a batch incubation study of RIP-G Tg islet. The insulin secretion from isolated islets of RIP-G Tg was indistinguishable from that of nontransgenic littermates. This finding indicates that insulin secretion was not affected by overexpression of ghrelin transgene *in vitro* but was affected *in vivo*. The different observations *in vitro* and *in vivo* may be explained by dilution of ghrelin produced by transgene with the incubation buffer. Alternatively, suppression of insulin secretion of RIP-G Tg was not due to the effect of desacyl ghrelin on